Impact of Atmospheric Rivers on Future Poleward Moisture Transport and Arctic Climate in EC-Earth2

Kolbe, M.; Sonnemans, J. P.J.; Bintanja, R.; van der Linden, E. C.; van der Wiel, K.; Whan, K.; Benedict, I.

Published in:
Journal of Geophysical Research: Atmospheres

DOI:
10.1029/2023JD038926

JGR Atmospheres

RESEARCH ARTICLE
10.1029/2023JD038926

Impact of Atmospheric Rivers on Future Poleward Moisture Transport and Arctic Climate in EC-Earth2

M. Kolbe[1], J. P. J. Sonnemans[2], R. Bintanja[1,3], E. C. van der Linden[3], K. van der Wiel[3], K. Whan[3], and I. Benedict[2]

[1]Faculty of Science and Engineering, Energy and Sustainability Research Institute Groningen, University of Groningen, Groningen, Netherlands, [2]Meteorology and Air Quality Group, Wageningen University and Research (WUR), Wageningen, Netherlands, [3]Royal Netherlands Meteorological Institute (KNMI), De Bilt, Netherlands

Key Points:

- The additional poleward moisture transport in warmer climates is almost exclusively due to atmospheric rivers (ARs)
- Higher atmospheric moisture levels are dominant in setting future AR increases, while dynamical changes are of secondary importance
- The interannual variability of ARs in local Arctic regions is closely related to the mid-latitude jet position and speed to the southwest

Correspondence to:
M. Kolbe,
m.kolbe@rug.nl

Citation:
Kolbe, M., Sonnemans, J. P. J., Bintanja, R., van der Linden, E. C., van der Wiel, K., Whan, K., & Benedict, I. (2023). Impact of atmospheric rivers on future poleward moisture transport and Arctic climate in EC-Earth2. *Journal of Geophysical Research: Atmospheres*, *128*, e2023JD038926. https://doi.org/10.1029/2023JD038926

Received 21 MAR 2023
Accepted 3 SEP 2023

Abstract

Alongside mean increases in poleward moisture transport (PMT) to the Arctic, most climate models also project a linear increase in the interannual variability (IAV) with future warming. It is still uncertain to what extent atmospheric rivers (ARs) contribute to the projected IAV increase of PMT. We analyzed large-ensemble climate simulations to (a) explore the link between PMT and ARs in the present-day (PD) and in two warmer climates (+2 and +3°C compared to pre-industrial global mean temperature), (b) assess the dynamic contribution to changes in future ARs, and (c) analyze the effect of ARs on Arctic climate on interannual timescales. We find that the share of AR-related PMT (ARPMT) to PMT increases from 42% in the PD to 53% in the +3°C climate. Our results show that the mean increases in AR-frequency and intensity are mainly caused by higher atmospheric moisture levels, while dynamic variability regulates regional ARs on an interannual basis. Notably, the amount of ARs reaching the Arctic in any given region and season strongly depends on the regional jet stream position and speed southwest of this region. This suggests that future changes in dynamics may significantly amplify or dampen the regionally consistent moisture-induced increase in ARs in a warmer climate. Our results further support previous findings that positive ARPMT anomalies are profoundly linked to increased surface air temperature and precipitation, especially in the colder seasons, and have a predominantly negative effect on sea ice.

Plain Language Summary

With ongoing global warming, the amount of moisture transported to the Arctic—and its interannual variability (IAV) (or year-to-year fluctuations)—will increase. While the former can be explained by a higher water holding capacity of the atmosphere, the cause of the latter is still uncertain. In this study, we link the IAV of poleward moisture transport (PMT) to atmospheric rivers (ARs), which are long narrow zones of relatively high water vapor content. Using a fully coupled global climate model, we detected ARs in a present-day and two warmer climates. We find that the vast majority of the future increase in PMT is caused by more frequent and intense ARs. While the increase in ARs is largely caused by higher moisture levels, our results also point to a dynamic influence. For example, a regional poleward shift and increased speed of the jet stream is associated with more ARs to the northeast. We also see significantly higher surface temperature and precipitation rates near regions of anomalously high AR activity in all seasons, and a predominantly negative response of sea ice to ARs. These linkages persist in a warmer climate, implying an increase in AR-related rainfall and the intensity of high-temperature events.

1. Introduction

Multiple studies have recently linked the increased presence of atmospheric rivers (ARs) to enhanced Arctic warming, sea ice loss, and precipitation extremes (e.g., Barrett et al., 2020; Hegyi & Taylor, 2018; Komatsu et al., 2018; Nash et al., 2018; Vázquez et al., 2018). Due to their potentially severe impacts on Arctic communities and ecosystems, there is large interest in determining the processes behind years of high AR occurrences and intensity. While in some regions ARs can be of benefit (e.g., by supplying water to dry areas in the mid-latitudes), Arctic ARs are mainly associated with negative impacts: flooding of Arctic communities (Bachand & Walsh, 2022), melting of the Greenland Ice Sheet (GrIS) (Mattingly et al., 2018, 2023; Neff, 2018; Wang et al., 2020), sea ice loss (Gimeno et al., 2015; Hegyi & Taylor, 2018; Wang et al., 2020), or dust transport from the subtropics (D. Francis et al., 2018, 2022) which may further enhance melting through ice albedo changes. Mattingly et al. (2018, 2023) showed that especially strong summer ARs are responsible for strong melt events in the ablation zone and are often associated with foehn events. Meanwhile, the authors also stress that Arctic ARs can supply protective snow mass in other areas, especially in colder months. A positive effect of ARs on surface mass balance and sea ice growth/protection has also been suggested by other studies (Light et al., 2022; Nghiem et al., 2016; Stroeve et al., 2022; Webster et al., 2019; P. Zhang et al., 2023). In the absence of a strict physical definition of what exactly defines ARs, they commonly refer to low-tropospheric long narrow zones of relatively high water vapor content. Often, they are associated with cyclonic and anti-cyclonic activity and net moisture transports from lower to higher latitudes nested in large-scale circulation patterns (Guo et al., 2020; Rutz et al., 2014; Woods et al., 2013; Z. Zhang et al., 2019; Zhu & Newell, 1998). Compared to the frequent and intense AR occurrence at lower latitudes, the number of ARs reaching the relatively dry and cold Arctic is small. However, a number of studies have revealed a significant increase in Arctic ARs in response to global warming, mainly owing to the expected increase in moisture alongside higher temperatures, following the Clausius-Clapeyron relation (Allan et al., 2014; Espinoza et al., 2018; O'Brien et al., 2022; P. Zhang et al., 2021).

Next to thermodynamic causes, Sousa et al. (2020) and P. Zhang et al. (2021) attribute the increase in Arctic ARs to a poleward shift of the polar jet stream related to both thermodynamic and dynamic changes. While the cause of this poleward shift is still debated, most studies attribute it to a tropical ocean warming-related shift of the sinks or sources of Rossby waves (Chen & Held, 2007; Kidston & Gerber, 2010; Rivière, 2011; Tandon et al., 2013; Wu et al., 2011). The signal of this poleward shift (linked to ocean warming) is not very strong and inconsistent across climate models, partly because Arctic sea ice loss counteracts the response by favoring an equatorward shift of the jet stream (Ma et al., 2021; Peings & Magnusdottir, 2014; Screen et al., 2022, 2013; Smith et al., 2022). Screen et al. (2022) suggested that the equatorward shift—caused by a sea ice loss-induced decreased meridional temperature difference in the lower troposphere—wins over the poleward shift if it is constrained by observations. In most current global climate models (GCMs), however, the sea ice signal is (too) weak, causing the poleward shift to dominate (Barnes & Screen, 2015; Hall et al., 2015; Payne et al., 2020; Yim et al., 2016). This may partly contribute to the general increase in simulated Arctic ARs, which are very sensitive to the mean position of the storm tracks.

It is less clear how the interannual variability (IAV) of Arctic ARs (e.g., increased AR-IAV or variability of mean AR pathways) responds to the interplay of thermodynamic and dynamic changes. Overall, the response of AR variability to the combination of these regional and large-scale mean changes is poorly studied. Until now, years with increased moisture intrusions into the Arctic have been linked to anomalous pressure systems in the vicinity of AR-pathways, which favor the river-shaped intrusions and are often linked to large-scale planetary waves (Bao et al., 2006; B.-M. Kim et al., 2017; H.-M. Kim & Kim, 2017; Komatsu et al., 2018; Papritz & Dunn-Sigouin, 2020; Woods et al., 2013). For example, pronounced ridge-trough patterns during negative phases of the North Atlantic Oscillation (NAO) allow ARs to reach western Greenland (C. Liu & Barnes, 2015; Neff, 2018), while positive phases of the NAO have been associated with increased ARs over northern and western Norway (I. Benedict, Ødemark, et al., 2019). These studies suggest that teleconnection patterns can greatly influence ARs in distinct Arctic regions. It is likely that more large-scale patterns such as the Arctic Oscillation may have an Arctic-wide impact, but so far there is no clear evidence for a significant Arctic-wide increase in ARs associated with any large-scale mode of climate variability.

Based on the Coupled Model Intercomparison Project (CMIP) 6 projections, Ma and Chen (2022) have further concluded that winter ARs over the Northern Pacific are strongly influenced by tropical sea surface temperature forcing, while ARs over the Northern Atlantic mainly depend on the internal variability of the atmosphere. Studies on future Arctic AR activity based on GCMs mainly address changes in the mean state of AR characteristics instead of drivers of IAV, focus on a particular season, or do not cover the entire Arctic region (Gao et al., 2015; Payne et al., 2020; Shields & Kiehl, 2016; Warner & Mass, 2017; Warner et al., 2015). Non-AR-related Arctic studies discussing future climates point toward a considerable increase in the IAV and number of extreme rainfall and melt events over the Arctic (Bogerd et al., 2020; C. Liu & Barnes, 2015; van der Wiel & Bintanja, 2021), which could be severely affected by fluctuations of annual AR occurrences. The simulated increase in Arctic precipitation IAV has previously been linked to the respective increase in the IAV of poleward moisture transport (PMT) (Bintanja et al., 2020; Bogerd et al., 2020; Skific et al., 2009a, 2009b). While the increase in mean PMT was found to mainly occur due to enhanced atmospheric moisture levels following atmospheric warming, the precise causes of the IAV increase are still uncertain (Bintanja et al., 2020; Bogerd et al., 2020; X. Zhang et al., 2013). Similar to the lack of knowledge concerning future AR-IAV, one of the main reasons for this is that PMT-IAV is largely effected by dynamic changes of the atmosphere and therefore sensitive to changes of the location of the jet stream and characteristics of storms reaching the Arctic. There is no established consensus

10.1029/2023JD038926

around the future of planetary-scale climate modes and the synoptic scale circulation, which by default are chaotic in nature and sensitive to climatic changes (Hall et al., 2015; Payne et al., 2020; Tan et al., 2020). The combined increase of mean and IAV of PMT translates into an increased intensity of extreme events in the Arctic (Bintanja & Selten, 2014; Pendergrass et al., 2017; van der Wiel & Bintanja, 2021), making it crucial to consider changes in variability.

This study examines both mean and IAV changes of the intensity and frequency of Arctic ARs. Variability is generally best identified over relatively long time periods or stable climate conditions without strong changes in mean trends. In order to robustly define IAV changes from the present-day (PD) to future climates, we therefore assess ARs in large-ensemble 5-year runs branched from three different periods of the EC-Earth2.3 RCP8.5 scenario. These three climate runs represent the present-day climate (hereafter PD), as well as a +2°C and a +3°C warmer than the pre-industrial (PI) climate as further described in Section 2.1. By calculating ARs for the future climates in two different ways (see Section 2.2), we aim to separate the thermodynamic (moisture-induced) from the dynamic (circulation-induced) effect. With this distinction, we are able to assess whether changes in AR(-IAV) are dominantly caused by shifts in wind patterns or by increased integrated water vapor levels. As we foresee both regional and seasonal non-homogeneity in the change of ARs and their driving mechanisms, we further distinguish between different seasons, and define the AR responses for four different Arctic sectors, as described in Section 2.2. The first part of this work (Section 3.1) discusses future changes in the relation between ARs and PMT, while the second part (Section 3.2) addresses the dynamical influence as well as seasonal and regional differences in these AR(-IAV) changes. Finally, Section 3.3 focuses on the relation between ARs and Arctic surface air temperature (SAT), precipitation (PR), and sea ice concentration (SIC).

2. Methodology

2.1. Data

We use three different EC-Earth2.3 large ensembles to investigate AR dynamics in present and future climates. Three initial-condition large ensembles were branched off from a 16-member historical + RCP8.5 experiment. A more detailed explanation of the construction of the large ensembles is given in van der Wiel et al. (2019). EC-Earth is a GCM based on the atmospheric integrated forecast system of ECMWF, coupled to an ocean model (Nucleus for European Modeling of the Ocean) with modules for sea ice (Louvain-la-Neuve, LIM2) and land components (Tiled ECMWF Surface Exchanges over Land incorporating land surface hydrology, HTESSEL) (Hazeleger et al., 2012). To contend with a cold bias over the Arctic region (Koenigk et al., 2013), the PD ensemble uses the model period 2035–2039 (experiment referred to as PD). The simulated global mean surface temperature (GMST) of this period best matches the observed GMST from 2011 to 2014. The two future climate scenarios are based on a GMST increase of 2°C relative to PI (2062–2066 equivalent) and a GMST increase of 3°C relative to PI (2082–2086 equivalent). Each climate simulation consists of 2,000 simulated years of global, daily data at 1.125° × 1.125° resolution for the atmosphere (van der Wiel et al., 2019). For the seasonal analysis, we had to omit 1 year of each 5-year run (the first year for DJF, and the fifth year for remaining seasons), resulting in 1,600 years for each season and climate. To detect ARs and calculate PMT, we obtained the daily specific humidity and the wind speed in zonal and meridional directions at four pressure levels (1,000, 850, 500, 200 hPa) from each climate ensemble. In addition, SAT, PR, and SIC are analyzed to assess the impact of ARs on Arctic climate indicators.

To validate the model data for the PD climate, we used monthly ERA5 reanalysis fields from 2005 to 2020 (Hersbach et al., 2020) and compared all variables in use here. As ERA5 has a higher spatial resolution of 0.25°, we regridded the field to the EC-Earth grid (1.125° × 1.125°). Validation results are discussed in Section 2.5.

2.2. Detection of Arctic ARs

The first AR detection criteria a northward directed meridional IVT-component and a minimum length/width ratio of 2 (Guan & Waliser, 2015). We defined the length as the maximum extension of an AR object, while the width is defined by the object surface area divided by the length. To be classified as an Arctic AR, the AR-pathway should cross 70°N.

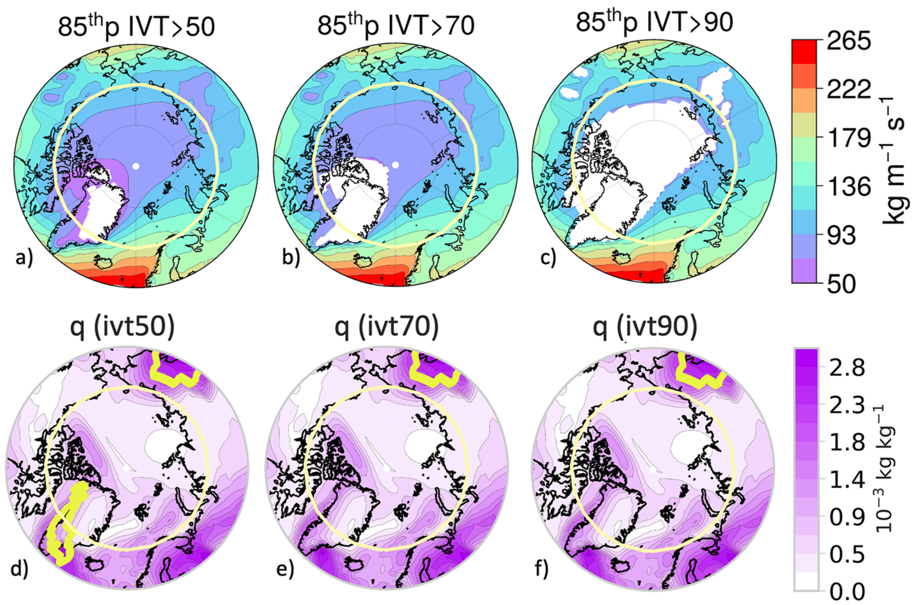

Figure 1. (a–c) Present-day integrated water vapor transport (IVT) >85th percentile in the EC-Earth runs, plotted behind three different masks indicating the effect of the minimum IVT thresholds. (d–f) Specific humidity from a random EC-Earth member (in January) including an Arctic atmospheric river detected only with the lowest threshold (yellow outline over Greenland).

Generally following the detection algorithm from Rutz et al. (2014), we calculated ARs based on ERA5 and the three different EC-Earth climates. For each grid point, we first calculated the integrated water vapor transport (IVT) as:

$$IVT = -\frac{1}{g}\int_{p_0}^{p_1} q\mathbf{V}dp, \tag{1}$$

where g is the gravitational acceleration (m s^{-2}), q is the specific humidity (kg kg^{-1}), $\mathbf{V}$ is the horizontal wind vector (m s^{-1}), consisting of a u and v component, and p_0 (p_1) is the surface pressure (upper boundary) level in hPa. We integrated from 200 to 1,000 hPa, using the 1,000, 850, 500, and 200 hPa pressure levels. Based on a sensitivity analysis with ERA5, we did not find significant differences when calculating IVT using 50 levels from 1,000 to 300 hPa instead of the four levels in this study, from which we assume sufficient accuracy of our IVT-calculation.

We define local IVT thresholds based on the IVT climatology to compute ARs. While most of the detection algorithms covered in latest reports of the Atmospheric River Tracking Method Intercomparison Project (ARTMIP) agree on a minimum AR length threshold of 2,000 km (Collow et al., 2022; Ralph et al., 2004), there is higher disparity in the IVT-thresholds across global AR studies. This inconsistency should not be avoided according to Rutz et al. (2019) and Shields et al. (2018), as every study addresses a specific question. However, the ARTMIP community suggests to include a sensitivity analysis by conducting AR calculations with slight adjustments to the algorithm. In addition to the commonly used grid-point-based IVT >85th percentile threshold, we therefore decided to apply three varying minimum thresholds of 50, 70, and 90 kg m^{-1} s^{-1} to detect Arctic ARs. These minimum thresholds only take effect when the local 85th percentile is met, which is illustrated for the PD in Figures 1a–1c. Based on our research objective and in order to be consistent with Guan and Waliser (2015) and Nash et al. (2018), we focus our analysis using the lowest minimum IVT threshold for the PD ARs, that is, 50 kg m^{-1} s^{-1} (however note that unlike Nash et al., 2018, we calculate ARs considering both the zonal and meridional wind component, which may cause differences in the amount of AR-related PMT [ARPMT]). Using 50 kg m^{-1} s^{-1} as a minimum IVT threshold allowed us to include PD ARs with slightly lower moisture transport but potentially strong effects on the usually dry Arctic climate. Figures 1a–1c show the effect of the different thresholds, where the mean IVT of the PD climate is plotted behind a mask of the respective minimum thresholds. This illustrates the regions where the minimum thresholds come into effect in the PD runs. The lower panel (d–f)

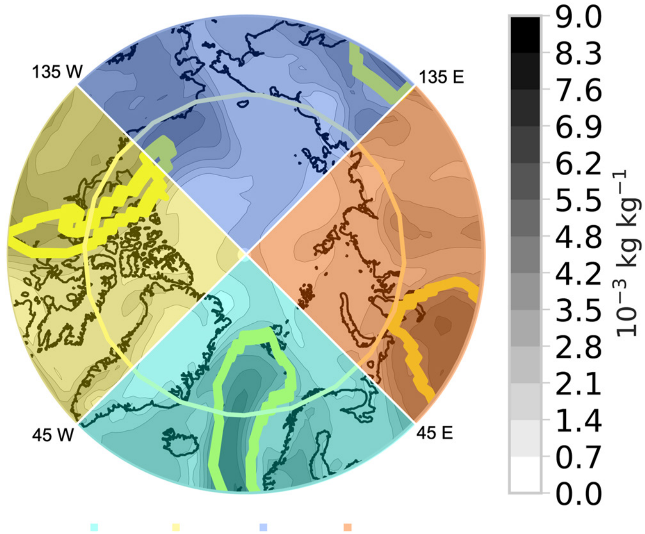

Figure 2. Illustration of the division of the Arctic region into the Atlantic (cyan), the Eurasian (orange), the Pacific (dark blue), and the Canadian (yellow) sector. Pictured is an example of two atmospheric rivers (ARs) reaching the Arctic region in present-day EC-Earth, superimposed on the moisture field at 850 hPa. The other ARs in the Eurasian and Pacific sectors are not included in this study (only to visually demonstrate the origins of ARs) as they do not pass 70°N.

illustrates an example of a winter AR only detected with the 50 kg m^{-1} s^{-1} minimum threshold, highlighting the cold and dry GrIS as one of the main regions affected by the choice of threshold. On this particular day, the IVT value of the AR over the GrIS is between 50 and 70 kg m^{-1} s^{-1}. Featured is also the tip of a detected AR over East Siberia excluded from our study as it does not cross 70°N.

For detecting ARs in the future climates, we used two different techniques:

1. To study the absolute changes in ARs, we preserved the PD thresholds to detect ARs in a +2°C and +3°C warmer than PI climate (referred to as 2C and 3C hereafter). According to the classification provided by O'Brien et al. (2022), this choice of threshold falls under the category of "fixed relative" methods, implying that the IVT value to be exceeded is relative to the location, but fixed in time.
2. To study dynamic-sensitive AR changes unrelated to increased moisture levels, we recalculated potential future ARs using a "relative" method (referred to as r2C and r3C hereafter). Here, we calculated and used the climate-specific local IVT thresholds while retaining the minimum thresholds as described above. Due to increased moisture levels in the warmer climates, the resulting 85th percentile thresholds are thus higher, meaning that detected ARs in the r2C and r3C runs are more sensitive to dynamic changes. As almost all local 85th percentiles in the future climates exceed 50 kg m^{-1} s^{-1} (not shown), we base our analysis on dynamic-sensitive future ARs detected with the 70 kg m^{-1} s^{-1} minimum threshold, where the regions affected by the minimum threshold are very similar (Figure A1). This allows for a fair comparison of differences in the dynamic changes of ARs (we found that if we used the 50 kg m^{-1} s^{-1} minimum threshold, there was an exceptional AR increase over the region in Greenland, as the minimum threshold criteria only had to be met in the PD climate).

2.3. Quantification of (AR-Related) PMT and AR-Frequency

To clearly distinguish PMT from equatorward moisture transport (EMT) along 70°N, we used the PMT calculation from Bengtsson et al. (2011):

$$PMT = -\frac{1}{g}\oint_L \int_{p_0}^{p_1} q\mathbf{V_n} dp dl, \tag{2}$$

where g is the gravitational acceleration (in m s^{-2}), L represents the 70°N latitude band, p_0 (p_1) is the surface pressure (upper boundary) level, q is the specific humidity (kg kg^{-1}), $\mathbf{V_n}$ the meridional wind across latitude L (in m s^{-1}), and l the latitude (between 70°N and 90°N). In addition to quantifying PMT (only poleward), EMT (only equatorward, i.e., negative PMT), and ARPMT (PMT across the part of the 70°N latitude band within AR-shapes), this method also allowed us to determine respective differences across longitudes along 70°N. AR-intensity is then defined as the amount of PMT within ARs at the 70°N latitude band.

We define AR-frequency as the amount of AR-shapes reaching 70°N on any given day (e.g., 2 ARs in Figure 2). ARs that last 2 days are therefore counted twice (if they still meet all AR detection criteria).

2.4. Division of the Arctic Region Into Sectors

As shown in previous work on Arctic moisture transport, ARs typically follow favorable pathways such as the Atlantic or Pacific Ocean basins (e.g., Nash et al., 2018; Vázquez et al., 2018). Here, a substantial number of ARs also reach the 70°N latitude band from continental areas in addition to the common ocean pathways. Because the main drivers of ARs in different regions may evolve differently toward a warmer climate, we

10.1029/2023JD038926

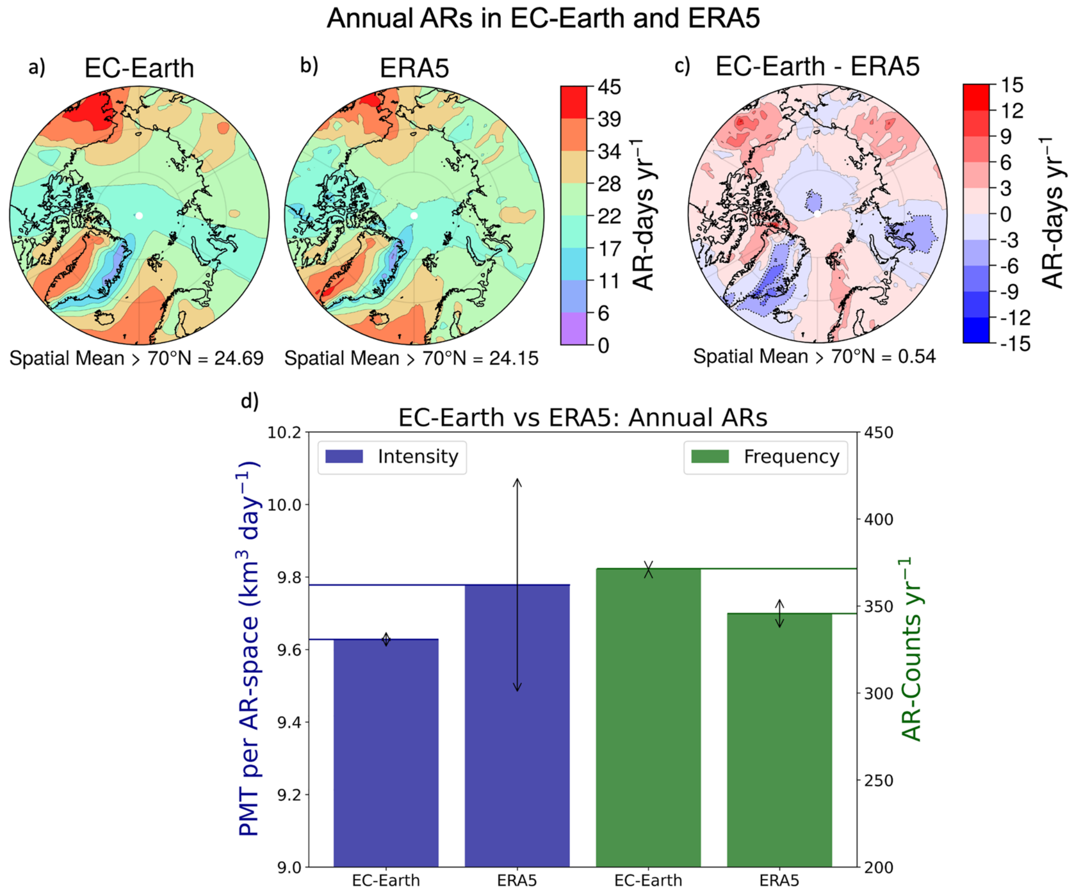

Figure 3. Annual mean atmospheric river (AR)-days in EC-Earth (a) and ERA5 (b). (c) Spatial mean difference of annual AR-days: EC-Earth-ERA5 (red = more AR-days in EC-Earth). (d) Mean intensity (poleward moisture transport per AR) and frequency (counted ARs per year, including duplicates for multi-day ARs) in EC-Earth (present-day run) and ERA5 (2005–2020). Vertical gray lines represent the 95th confidence intervals (for EC-Earth frequency only [370.5, 372.4]).

present AR-IAV changes on a sector basis. We divide the Arctic into four sectors separated by four meridians (45°E, 45°W, 135°E, 135°W) as shown in Figure 2, exemplifying 2 ARs reaching the Arctic in late May, one in the Canadian sector and one in the Atlantic sector. Although the Canadian AR also reaches the Pacific sector, we only assign one sector to each AR (the one with the most amount of AR area north of 70°N). The 2 ARs in the other sectors have been detected based on their IVT and shape, but are not counted as Arctic ARs, as they do not cross 70°N (i.e., they are excluded from our statistics but serve as visual demonstrations of AR origins).

2.5. Validating ARs in EC-Earth With ERA5

Generally, there is good agreement between the frequency and intensity of ARs in EC-Earth and ERA5 (Figure 3d). ARs in ERA5 detected during 2005–2020 carry slightly more moisture (9.79 kg kg^{-1}) than those detected in the EC-Earth ensembles (9.63 kg kg^{-1}), while EC-Earth tends to detect more ARs on an annual basis (371 ARs in EC-Earth vs. 346 ARs in ERA5). Still, both are of similar magnitude given the common large variance of AR characteristics (O'Brien et al., 2022). As shown in Figure 3c, EC-Earth detects slightly less ARs over the GrIS, the West Atlantic, the Kara Sea, and the Pacific Central Arctic than ERA5, while more ARs are detected over the North Atlantic and lower latitudes of most continental areas north of 70°N. Although this study only assesses ARs passing 70°N, we include the latitudes between 60°N and 70°N to visualize the pathway of Arctic ARs (the spatial mean still only refers to the area north of 70°N). When comparing AR-days of all grid points, EC-Earth detects 0.45 more AR-days per year than ERA5. In terms of spatial patterns and magnitude, these results are nearly identical across the three different minimum IVT thresholds (not shown).

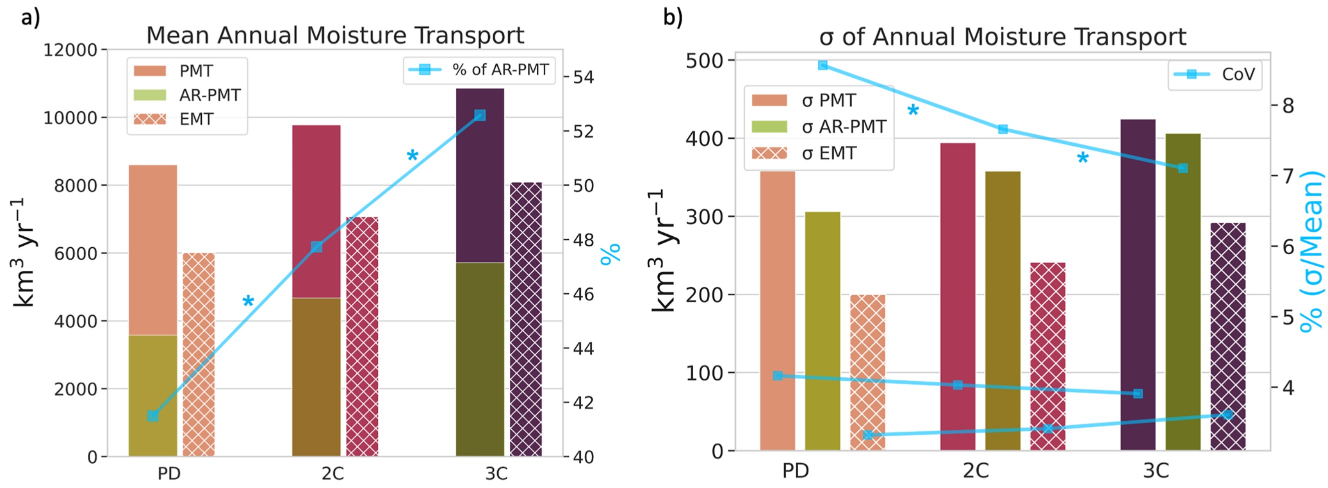

Figure 4. (a) Annually averaged poleward moisture transport (PMT), AR-related PMT (ARPMT), and equatorward moisture transport (EMT) in the present-day, +2°C warmer than PI (2C), and +3°C warmer than PI (3C) climates. The increase of AR-related PMT to total PMT is illustrated by the blue line, with the percentage of ARPMT displayed on the right *y*-axis. (b) Interannual variability (IAV) of PMT, ARPMT, and EMT in the three climates. The respective increases in IAV relative to the mean increase (coefficient of variation, CoV) are illustrated by the blue lines, with the percentage displayed on the right *y*-axis. The stars next to the CoV lines indicate that the change from climate to climate is significant (p-value of test <0.05).

Additionally, we compared the variables that impact or are associated with ARs (see Section 3.3: impacts of ARs on Arctic climate). Figure A2 shows the difference between EC-Earths and ERA5s average SAT, PR, and SIC. In brief, the difference in the temporal mean is small for all variables, while EC-Earth is cooler over Greenland and the Central Arctic Ocean and Pacific sector, but warmer over the majority of the Atlantic and Eurasian sector. Correspondingly, the slightly warmer (cooler) regions in EC-Earth exhibit higher (lower) PR and lower (higher) SIC.

3. Results and Discussion

For the majority of the study, we analyze future ARs detected using the "fixed relative" method (2C and 3C ARs) in order to focus on the absolute changes that occur from the PD to warmer climates. In Section 3.2, we further investigate future ARs detected using the "relative" method (r2C and r3C ARs) to study the contribution of dynamic changes to future ARs.

3.1. Changes in (AR-Related) PMT

In order to discuss climate-related AR-changes in the context of increased PMT, we first identify the spatial mean changes of moisture transport across 70°N. We note an increase in annual mean PMT toward warmer climates (Figure 4a), consistent with previous studies (Bintanja et al., 2020; Bogerd et al., 2020; P. Zhang et al., 2021). Furthermore, the relative percentage of ARPMT to total PMT increases by 11%, which is roughly consistent across all four seasons (Figures 5a, 5c, 5d, and 5g). The relative percentage of ARPMT is much higher in the warmer months (in all three climates), which is partly a side effect of our choice of an annually uniform IVT threshold. Nash et al. (2018) used seasonal-specific thresholds and still found that the share of Arctic ARPMT to total PMT is largest in summer. The increase in ARPMT/PMT ratio alongside an increase in mean PMT appears in all seasons, and indicates that the extra PMT is mainly caused by more frequent and/or more intense ARs. Annually averaged, 95% of the additional PMT from the PD to the 3C climate is transported through ARs (ΔARPMT/ΔPMT = 0.948). Obviously, this number is very sensitive to the AR definition: here, we refer to ARPMT in the 3C experiment, and thus, all relatively concentrated PMT plumes can easily exceed the IVT >85th percentile threshold of the PD climate and be counted as an AR.

Although PMT-IAV also linearly increases from the PD to the 3C climate (Figure 4b), the variability increase is moderate compared to that of the mean. This is demonstrated by a small (and insignificant) decrease in the coefficient of variation (CoV; standard deviation divided by the mean) of PMT from PD to warmer climates (blue

10.1029/2023JD038926

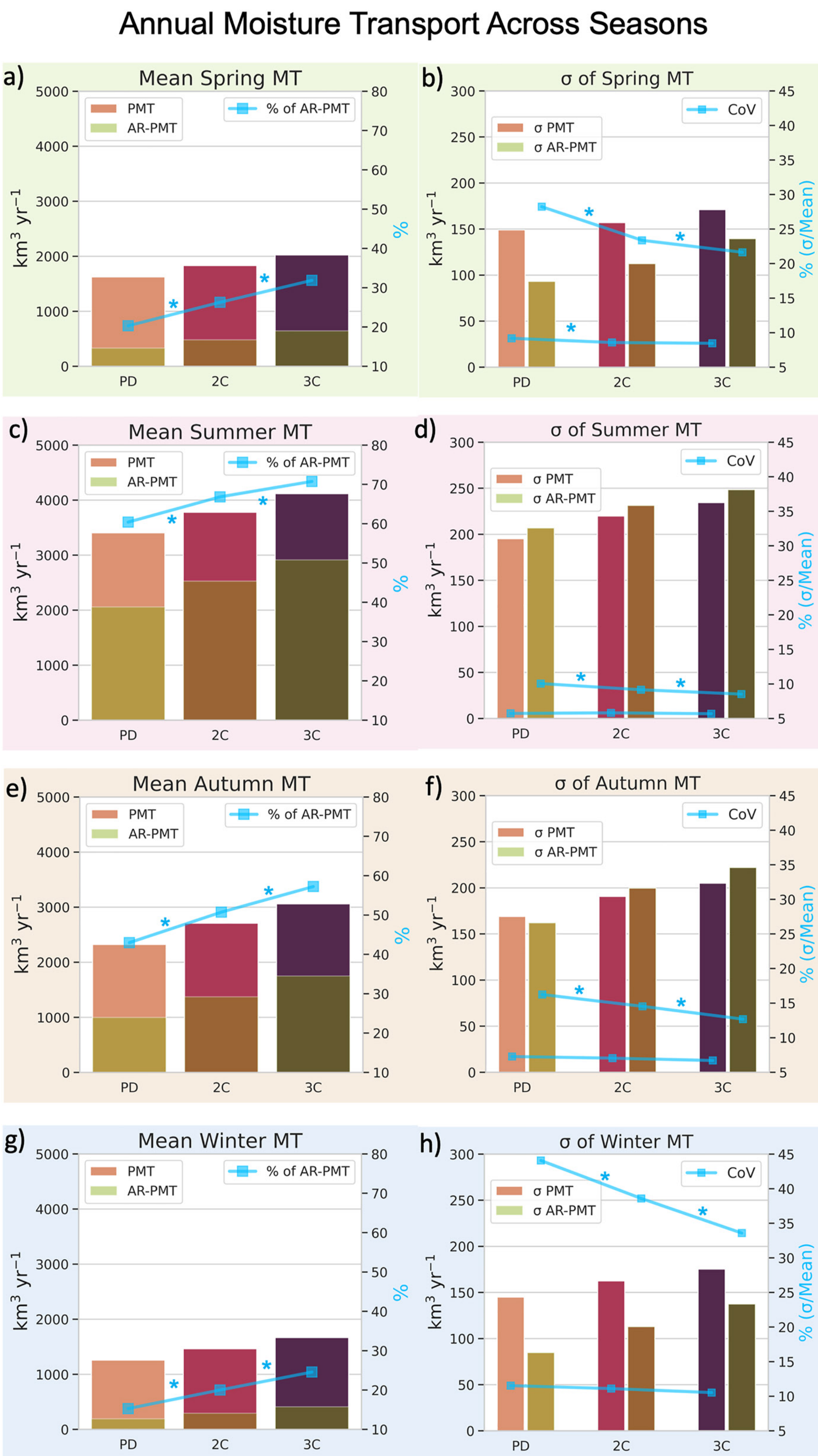

Figure 5. As in Figure 4, but on a seasonal basis and without equatorward moisture transport. (a, b) Spring (MAM). (c, d) Summer (JJA). (d, f) Autumn (SON). (g, h) Winter (DJF).

lines in Figure 4b). While the negative CoV trend of PMT is small and mainly insignificant in our simulations, it is present in all seasons, and even significant in spring (from PD to 2C; Figure 5b).

We compared our results to the simplified PMT calculation (area-averaged precipitation minus evaporation), which in contrast suggests a small disproportional increase in PMT-IAV relative to its mean (i.e., slightly increased CoV; not shown). We also calculated the change in PMT-IAV using 31 other CMIP6 models (SSP-5.8.5; not shown), which also project a small insignificant increase of variability, consistent with a CMIP5 study (Bintanja et al., 2020). The difference in the sign of the PMT CoV trend across different methods likely stems from the fact that the simplified PMT calculation assesses the net moisture to and from the Arctic, which thus does not distinguish poleward from EMT. This idea is supported by the slight increase in EMT (Figure 4b) in our simulations (which, however, is not significant at least on an annually averaged basis), and highlights the importance of strictly differentiating between the northward and southward component of moisture transport.

Our results thus suggest that the increase in (strictly northward) PMT-IAV is fairly weak and mainly a secondary effect of increased mean PMT. The CoV of AR-related PMT also decreases significantly, both annually (Figure 4b) and in all seasons (Figures 5b, 5d, 5f, and 5h), implying a more consistent, relatively less variable AR-associated moisture transport to the Arctic in warmer climates. This CoV decrease of ARPMT can thus explain the CoV decrease in total PMT, taking into account the high ARPMT-to-PMT share in warmer climates (Figure 4a).

To summarize, Arctic ARs transport nearly all additional poleward moisture in future climates, and their contribution to Arctic moisture transport becomes more consistent and relatively less variable. We found that ARPMT is slightly lower using the two higher thresholds (Figure A3), but the results were not qualitatively effected by this. So far, the AR changes toward the warmer climates are based on the simulations where the same moisture threshold as that for the PD detection is used. We will now also assess the climate-relative AR simulations (r2C and r3C) to investigate if the changes are at least partly dynamically driven. Additionally, we address whether the increase in AR-related PMT is caused by increased frequency or intensity of ARs.

3.2. Dynamic and Thermodynamic Changes of ARs and AR-IAV Across Seasons and Sectors

Based on the results above, this section addresses the following questions:

1. Where and when do ARs and AR variability increase most, and are these changes partly circulation-driven or due to higher moisture levels?
2. What increases more: the frequency or the intensity of ARs and AR variability?
3. Does the jet position (latitude) drive the IAV of Arctic ARs?

To address these questions simultaneously, we present regional and seasonal changes while introducing changes in the characteristics of ARs detected using climate-relative IVT thresholds (ARs in the r2C and r3C simulations).

3.2.1. Where and When Do ARs and AR Variability Increase Most, and Are These Changes Partly Circulation-Driven?

Here, we discuss dynamic and thermodynamic changes in the occurrence of ARs and their variability. The strongest increase in AR-days from the PD to the 3C climate occurs over the North Atlantic storm track region, the western GrIS, and Northwestern Canada (Figure 6b), where ARs are already most frequent (Figure 6a). North of 70°N, the occurrence of AR-days increases by 15 days per year (mainly in summer and autumn; Figures A4c and A4e), with up to 26 additional days over the North Atlantic. Most ARs reaching the deeper Arctic in warmer climates originate from the Atlantic sector (across the Norwegian Sea), which is in line with current trends (Vázquez et al., 2018), and applies to all seasons (Figure A4). These ARs are of particular importance, as, from a relative perspective, AR-days increase most over the Central Arctic Ocean (Figure 6c). In particular, ARs over the Northeast GrIS, as well as regions north of the Fram Strait and the Barents Sea occur more than twice as often in 3C compared to the PD climate. The Central Arctic is the region where the relative increase in specific humidity is strongest (Figure 7c), which increases the likelihood of fulfilling the detection criteria.

In fact, we do not find a substantial increase in annual mean Arctic AR-days if we adjust the IVT threshold (r3C experiment; Figure 6d), which further implies that the absolute increase is mainly moisture-driven. Rather, the dynamic response is mostly negative (fewer AR-days), especially over the GrIS. In r3C, there are up to 6 fewer

10.1029/2023JD038926

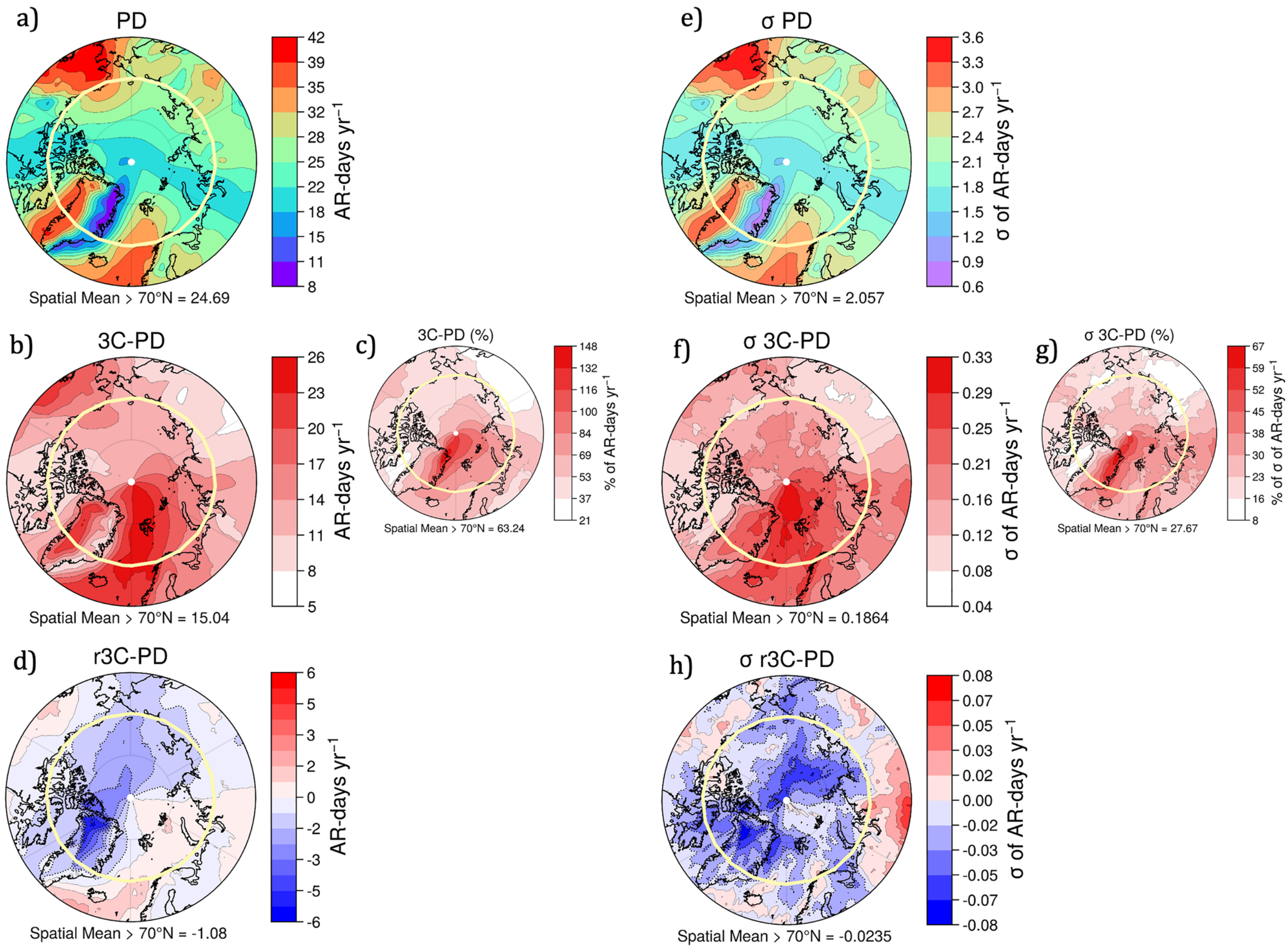

Figure 6. Left panel: Present-day annual atmospheric river(AR)-days per grid point (a), and their absolute increase toward the 3C climate (b). Side plot c shows this increase relative to the location. Panels (d) same as (b) but based on the r3C runs, thus representing differences in AR-days caused by mainly dynamic changes. Right panels (e–h): Same as left panel except for interannual variability (standard deviation of annual means).

AR-days over the GrIS and 2–3 fewer AR-days over the majority of the Arctic Ocean, except for the Atlantic sector. The wind components and the sea level pressure (SLP) change from the PD to the 3C climate indicate a strengthening of the Greenland Blocking High (GBH): while SLP decreases over the entire Arctic Ocean, it increases over the Central GrIS (Figure 7d), corresponding to a strengthening (weakening) of meridional winds east (west) of Greenland (Figure 7g). Although the regional patterns and changes in magnitude may be model-dependent, these trends have already been identified using observation-based data, and linked to enhanced summer and winter moisture transport to the GrIS (Barrett et al., 2020; Rimbu et al., 2007). In EC-Earth, the increase in Greenland blocking only occurs during winter and spring (Figures A4i and A4l), while in summer, we see a decrease (Figures A4j and A4k). As the majority of our ARs occur during summer (due to the annual mean IVT threshold), this can explain why the dynamic-induced annually averaged contribution to future ARs over Greenland is negative (Figure 6d). The annual mean zonal wind response in the warmer EC-Earth climate indicates an intensification of the North Atlantic storm tracks (in line with most GCMs as mentioned above), and decreased westerlies on the Pacific side (Figure 7i). The strength of meridional winds in the eastern part of the Pacific increases, but decreases in the western and the northern part of the Pacific Arctic Ocean sector (Figure 7g). These circulation changes toward warmer climates partly drive the dynamic-sensitive AR response (Figure 6d): fewer AR-days in the Pacific sector of the Arctic Ocean, and a weak increase (up to 2 more AR-days) over the Barents and Kara seas in the North Atlantic vicinity. However, this trend is dominated by the summer season, while we see fewer (more) AR-days in the Atlantic (Pacific) sector during winter in our r3C experiment

10.1029/2023JD038926

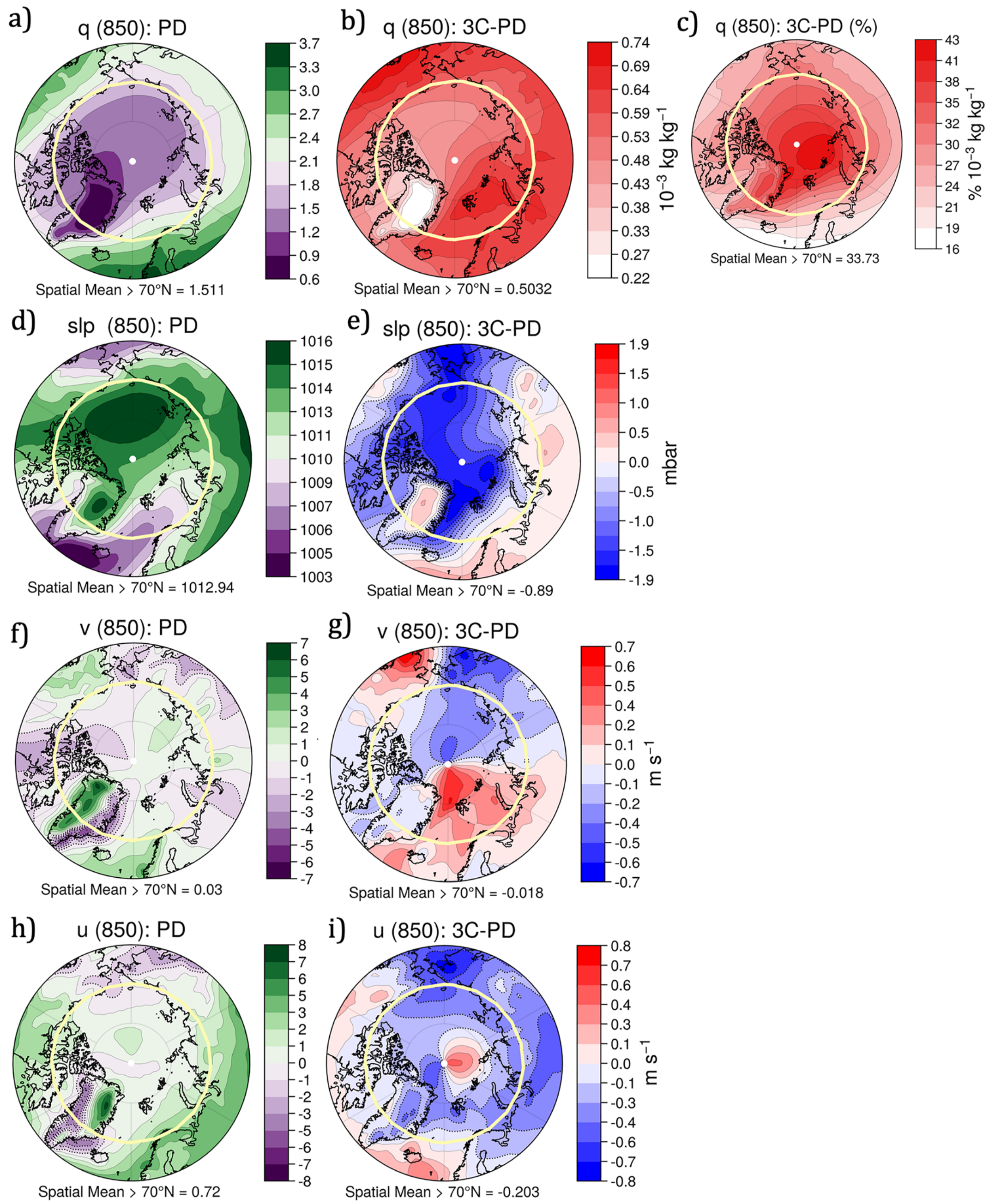

Figure 7. Present-day annual mean fields at 850 hPA of (a) moisture (q); (d) sea level pressure (SLP); (f) meridional winds (v); and (h) zonal winds (u), and the difference toward the 3C climate ((b, e, g, i), respectively). For the moisture field, the relative increase is shown in (c).

(Figure A4h). In Section 3.2.3, we analyze the relationship of ARs and atmospheric patterns on interannual time scales on a seasonal basis.

The spatial pattern of IAV of PD Arctic AR-days is closely related to the mean distribution, that is, regions with higher AR occurrences also show larger year-to-year fluctuations (Figure 6e). Likewise, the IAV of AR-days increases most over the Atlantic sector of the Central Arctic Ocean (Figure 6f). While the increase in mean AR-days is stronger over the west than over the east of Greenland, the variability increases most over the northeast (Figures 6b and 6f; dominated by summer and autumn, reversed in winter and spring—not shown). Especially from a local-% perspective, the IAV (and mean amount) of ARs strongly increases over the Northeast

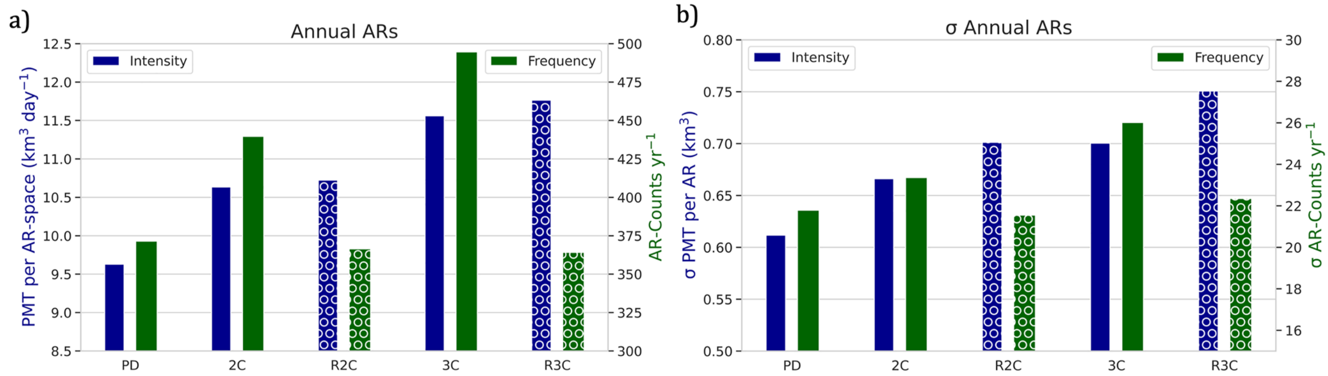

Figure 8. (a) Annually averaged intensity (PMT per AR, blue) and frequency (counted ARs, green) in a present-day (PD), +2°C warmer than PI (2C), and +3°C warmer than PI (3C) climate. Bars with white circles represent the respective indices for the relative (r2C and r3C) climate ensembles. (b) Same as (a) but for interannual variability, defined as the standard deviation of annual means.

GrIS (Figures 6c and 6g), where Mattingly et al. (2023) have recently attributed intense melting events with AR-induced foehn winds. Compared to the stronger relative mean increase of ARs across the entire Arctic (63% on average; Figure 6c), the local-% increase in IAV is moderate (28% on average; Figure 6g). This result aligns with the decrease in the CoV of ARPMT toward warmer climates (Figure 4b).

The reduced AR-day variability in response to global warming is partly caused by dynamic changes: in r3C, the IAV of AR-days is lower than at present in almost all Arctic regions (Figure 6h; but the difference is very small). It decreases most over Greenland and the Pacific sector of the Arctic Ocean (following the r3C mean—Figure 6d); however, it also over the Atlantic sector. While mean changes in the Arctic climate (e.g., increased PR and SAT) are mainly caused by local processes such as evaporation in response to sea ice loss, the IAV of Arctic climate variables is more sensitive to changes in atmospheric dynamics and lower latitudes (Bintanja et al., 2020; Bogerd et al., 2020; Gimeno-Sotelo et al., 2019; Higgins & Cassano, 2009).

To conclude, our simulations project an increase in absolute AR-days over the entire Arctic in a warmer climate. Even over regions such as the GrIS, where we see a reduction in wind transport associated with increased blocking, the increase in moisture levels result in increased AR-days, with severe potential impacts on surface melting (Mattingly et al., 2018; Neff, 2018). While we highlight strong seasonal differences, the dynamic response of Arctic AR occurrences to global warming is moderate overall. We note a small dynamic-induced increase (decrease) in future ARs that reach the Arctic from the Atlantic (Pacific) sector, which would occur under the assumption of a poleward shift of the North Atlantic storm tracks (Barnes & Screen, 2015; Hall et al., 2015; Payne et al., 2020; Yim et al., 2016). Although the IAV of AR-days increases across the entire Arctic, we find that this increase is weak compared to that of the mean. This result aligns with the decreased CoV of ARPMT, and is likely a sign of the different processes governing mean versus IAV changes.

3.2.2. What Increases More: The Frequency or the Intensity of ARs and AR Variability?

In this part, we discuss future changes in the frequency and intensity of Arctic ARs. Although AR-intensity and AR-frequency are partly linked (higher moisture levels allow for more detected ARs), this analysis provides additional insights on the potential impact per AR. The results above already indicate an increase in AR-days, while higher humidity levels (Figure 7b) further suggest that most future ARs will also carry more moisture. As the IAV increase of AR-days is relatively weak compared to the mean increase (Figure 6), this section will reveal whether this is due to a decreased CoV of AR-frequency or AR-intensity (explained in Section 2.3), or both.

Figure 8a illustrates how both the intensity and frequency of Arctic ARs increase almost linearly from the PD over the 2C to the 3C climate. The intensity of ARs in the r2C and r3C simulations is not significantly higher than in the 2C and 3C climates, and the frequency of r2C and r3C ARs is even (negligibly) lower (366 and 364 ARs year^{-1}) compared to the PD level (371 ARs year^{-1}). In agreement with the previous findings, these results suggest that both the increased intensity and frequency in warmer climates are mostly a response to higher moisture levels instead of dynamic changes. The dynamic influence on increased IAV of AR-frequency is likewise minor (Figure 8b). However, we do note a significant increase in the IAV of AR-intensity in r2C and r3C compared

10.1029/2023JD038926

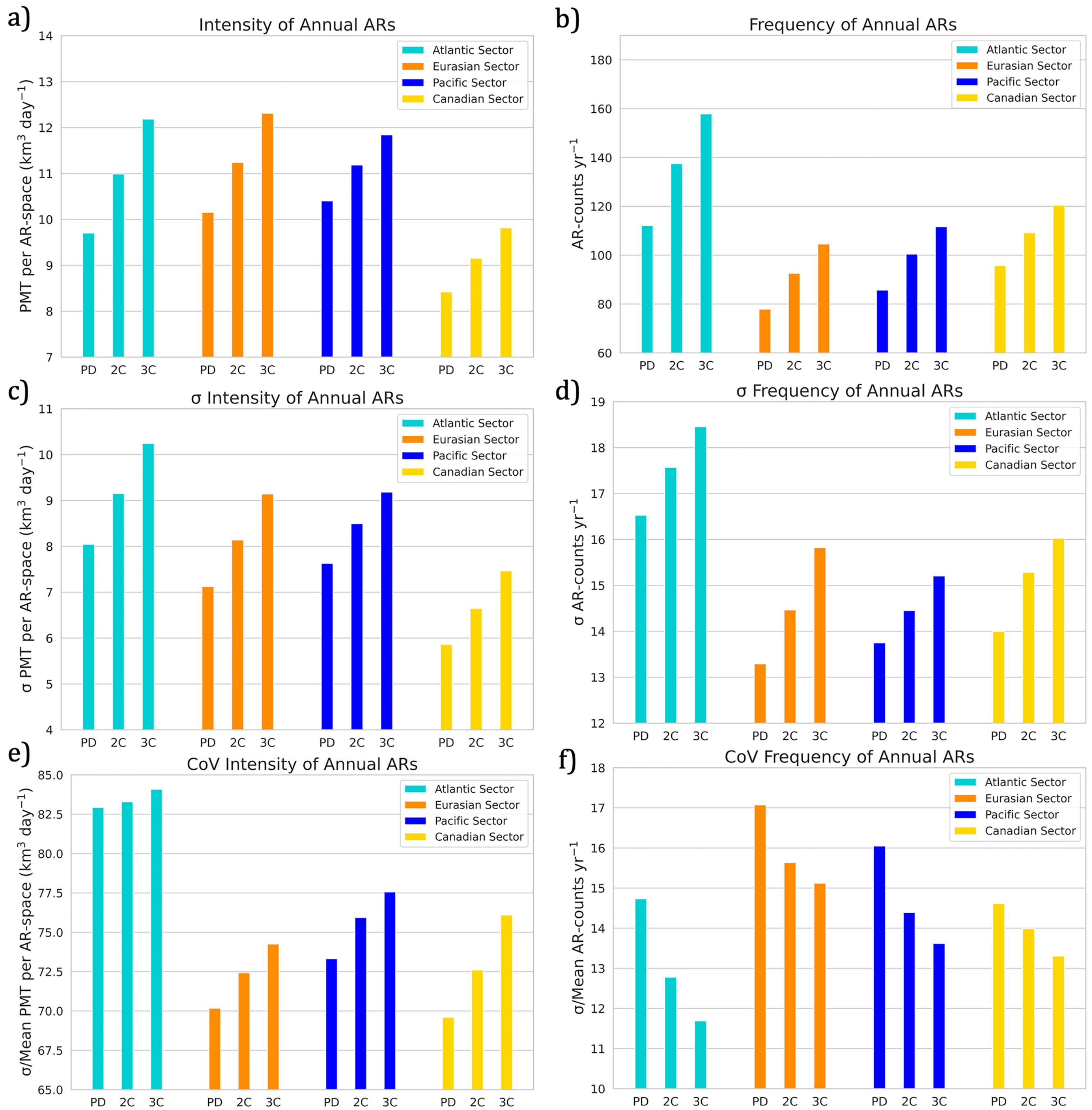

Figure 9. (a) Annually averaged intensity (poleward moisture transport [PMT] per atmospheric rivers (AR)), (a) and frequency (counted ARs, (b)) in the PD, 2 and 3C climates. (c, d) Same as (a, b) but for interannual variability (IAV, defined as the standard deviation of annual means). (e, f) IAV as in (c, d) scaled by the mean changes in (a, b).

to 2 and 3C, which suggests that the annually averaged transported moisture per AR in warmer climates partly depends on atmospheric dynamics. A reason for this may be that in 2 and 3C, variations of AR-intensity are lower because there are more (including weaker) ARs detected. Furthermore, these spatially averaged changes in intensity and frequency could be subject to compensations between different Arctic sectors.

The increases in intensity and frequency of ARs are of similar magnitude in all Arctic sectors (Figures 9a and 9b). To investigate frequency and intensity changes on regional scales, we focus on the four Arctic sectors (Figure 2). By scaling the changes in IAV by the mean changes of each sector (i.e., CoV), we examine whether increased

10.1029/2023JD038926

fluctuations in AR activity are only a result of increases in the mean. For these analyses, we only focus on the 2 and 3C ARs, as the r2C and r3C simulations indicate similar results in terms of the CoV patterns. In the PD climate, ARs from the Pacific sector are most intense, while ARs from the Atlantic sector are significantly more frequent. The relatively low intensity over the Atlantic and Canadian sectors is likely due to the low humidity in the vicinity of the cold GrIS. However, the intensity of Atlantic sector ARs significantly increases toward the 3C climate, reaching similar levels as those of Pacific sector ARs (Figure 9a). Despite the relatively low mean intensity of Atlantic sector ARs, the annually averaged amount of PMT per AR fluctuates most over the Atlantic sector (Figure 9c). This may be caused by years with many ARs over Greenland (lower mean intensity), alternating with years with few ARs over Greenland (higher mean intensity). Otherwise, the IAV of AR-intensity and frequency roughly corresponds to the respective mean states in each sector and likewise increases over all sectors (Figures 9c and 9d). The CoV changes emphasize the anomalously high IAV of AR-intensity over the Atlantic sector (Figure 9e), while the clearly reduced CoV of AR-frequency indicates that the number of ARs over the Atlantic sector is relatively constant compared to other sectors (Figure 9f). Most notably, the CoV of AR-frequency significantly decreases in all sectors toward warmer climates. Meanwhile, the CoV of AR-intensity significantly increases in all sectors.

These results reveal that the decrease in the CoV of ARPMT (Section 3.1; indicating more consistent ARPMT) is not caused by a decrease in the CoV of AR-intensity, but by AR-frequency (also shown by reduced AR-days, Section 3.2.1). In other words, the number of ARs reaching the Arctic becomes more consistent and relatively less variable. In contrast, the IAV in the intensity of future ARs increases disproportionately to the mean increase. This is crucial as it reveals that while ARs are getting significantly more consistent, there is increased uncertainty around the amount of moisture ARs carry in any given year (partly caused by increased sizes of future ARs). It is therefore of interest to examine the causes of years with anonymously high or low AR-related moisture transport to the Arctic, as discussed hereafter.

3.2.3. Does the Jet Position (Latitude) Drive the IAV of Arctic ARs?

Here, we examine whether the changes in jet stream location are linked to a change in AR activity, depending on the season and sector. Determining the relationship of jet stream latitude and AR activity on an interannual basis may further help to explain whether mean changes in ARs from the PD to a warmer climate are partly caused by jet stream shifts. This is of relevance, as the mean poleward shift of the jet stream in GCMs may be underestimated (Screen et al., 2022), potentially resulting in inaccurate AR-responses to warmer climates (including this study). On the other hand, the potential underestimation of future Arctic sea ice loss (Z. Liu et al., 2021; Notz & Community, 2020; Stroeve et al., 2012) and the atmosphere response simulated by GCMs (Smith et al., 2022) could imply an equivalent underestimation of the equatorward jet shift (Ma et al., 2021). Hence, studying the effects of jet latitude on Arctic ARs on an interannual basis provides information on both ends and offers a reference to different jet and AR scenarios.

To determine changes in the jet stream, we first average the zonal wind at 850 hPA, broadly following Woollings et al. (2010) (we use seasonal values, a fixed pressure level, and various sectors). The mean jet speed in each sector, season, and climate is then defined as the maximum westerly wind speed between 30° and 70°. The mean latitude of the jet is quantified by averaging these maximums over the latitudes. We also performed the same analysis using the method applied by Screen et al. (2022) and Zappa et al. (2018), which did not significantly affect results.

Figures 10a–10d show the mean jet latitude for the PD to the 3C climates, as well as the respective mean sea ice extents. In all seasons and most sectors, the shift of the mean jet latitude is minimal. The poleward shift toward warmer climates as found in some GCMs is only apparent in the Atlantic and Canadian sector during summer and autumn (Figures 10b and 10c). In all other seasons and sectors, the shift of the mean jet latitude is minimal, except for an equatorward shift of the winter and spring jet stream latitude over Northern Eurasia. Such spatial differences highlight that the weak jet stream response of the zonally averaged mean is partly a result of regional compensations. Furthermore, the weak mean response to future warming does not entail a lack of response, but may still fit into the picture of a more wavy and varying jet stream (J. A. Francis & Vavrus, 2015; Overland, 2021), which does not require a change in mean latitude. Regarding jet speed (Figures 10e–10h), we also find no significant spatially or seasonally consistent trends, although different choices in the sector division and size might yield stronger responses. In spite of weak mean changes, a consistent pattern is found in that all sector-specific poleward (equatorward) shifts are associated with increased (decreased) jet speeds.

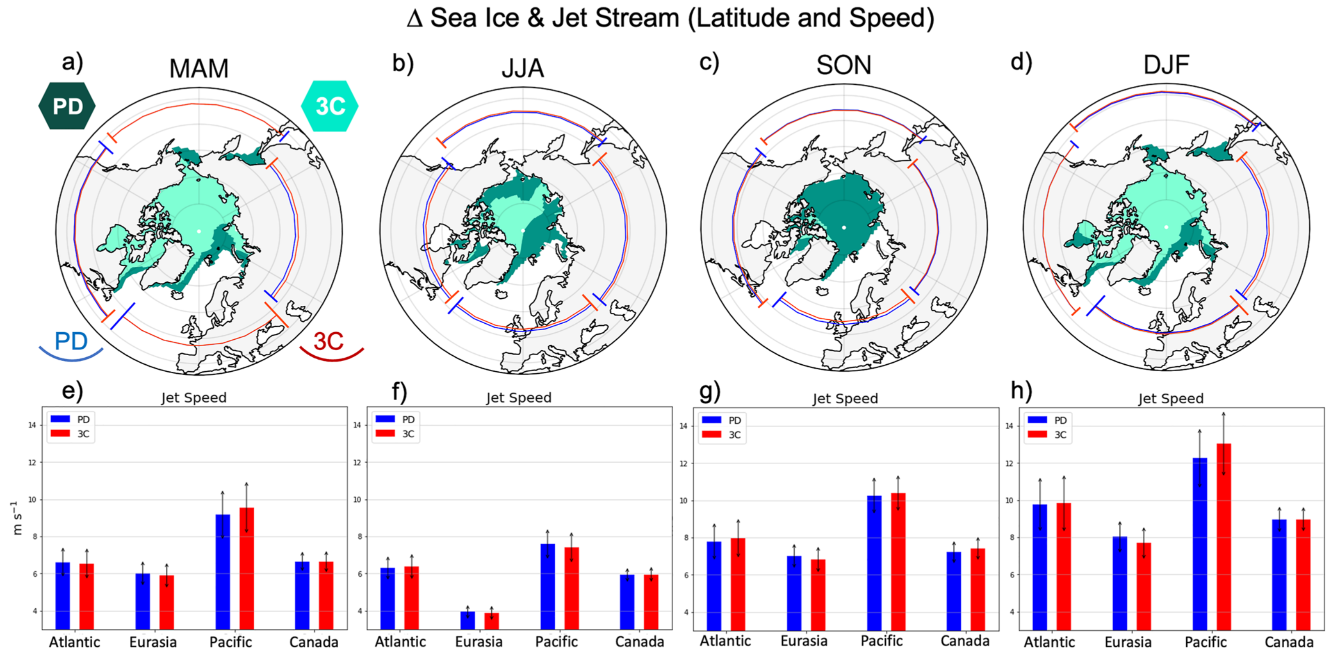

Figure 10. (a–d) Seasonal averages of the sea ice extent (>15%) and mean jet latitude in the four sectors, for the present-day (PD) and the +3°C warmer than PI (3C) climate. Vertical blue (red) lines on the left (right) of the mean jet latitudes represent the respective 95% confidence intervals. (e–f) Respective mean jet speed averaged intensity and 95% confidence intervals.

Next, we discuss whether the IAV of jet stream characteristics influences Arctic ARs. We find that in all regions, a poleward shift of the seasonal jet latitude is typically associated with more (less) ARs east (west) of the respective region (Figures 11a–11d). The reason for the decrease in ARs at the western side of each sector is partly caused by a concurrent increase in jet speed (Figures 11i–11l), forcing the poleward-oriented moisture further west than usual. Over the Pacific Ocean, anomalously higher jet speeds can reduce the amount of annual ARs over the entire sector by 5 less AR-days, and can instead force these ARs to reach Northern Canada (Figure 11k). The reason for why this pattern is less obvious over the Atlantic Ocean is likely due to the choice of our sector division (the Atlantic sector includes considerably more land regions with reduced wind speeds; Figures 10e–10h). Similarly, years in which the Canadian jet is stronger (and located further north) results in increased AR-days over the Atlantic (Figures 11d and 11l). Our results further suggest a comparable influence across sectors on ARs reaching the Arctic, implying that the net amount of ARs reaching the Arctic in any given year is influenced and likely compensated by regional differences in jet speed and latitude. These regional differences highlight the importance of examining jet sections rather than global mean jet properties.

In a +3°C warmer climate relative to PI, we find stronger regressions between jet stream latitude (Figures 11e–11h) and Arctic AR-days (Figures 11m–11p). To first degree, these higher regression coefficients are likely a by-product of an Arctic-wide increase in AR-days (Figure 6b). From this we can once more infer that the overall increase in Arctic ARs is not primarily caused by dynamic changes. That said, we find a warming-induced increase in the amount of grid points north of 70°N, which are significantly influenced by jet variations, indicating that the Arctic climate under continued warming will be more connected to the dynamics in lower latitudes. In other words, while the main increase in ARs in our 3C simulations is mainly a result of increased moisture (thermodynamic), the dynamic component is still required to transport the moisture to even higher latitudes. The assumption of a weak future poleward shift of the jet latitude in the Atlantic sector during summer and autumn (Figures 10b and 10c) would thus favor more ARs over the Barents and Kara Sea, and less ARs over Greenland. Such a pattern indeed appears in the dynamic AR-response to increased warming (Figure 6d), suggesting that the local trends in dynamic AR-responses are partly caused by a poleward shift of the Atlantic jet. The regressions showed very similar patterns across seasons (with strongest regressions in summer due to higher AR occurrences).

To summarize, we did not find significant changes in the mean location and speed of the jet stream (in agreement with most GCMs), apart from a slight poleward shift in warmer seasons in the Atlantic and Canadian sectors.

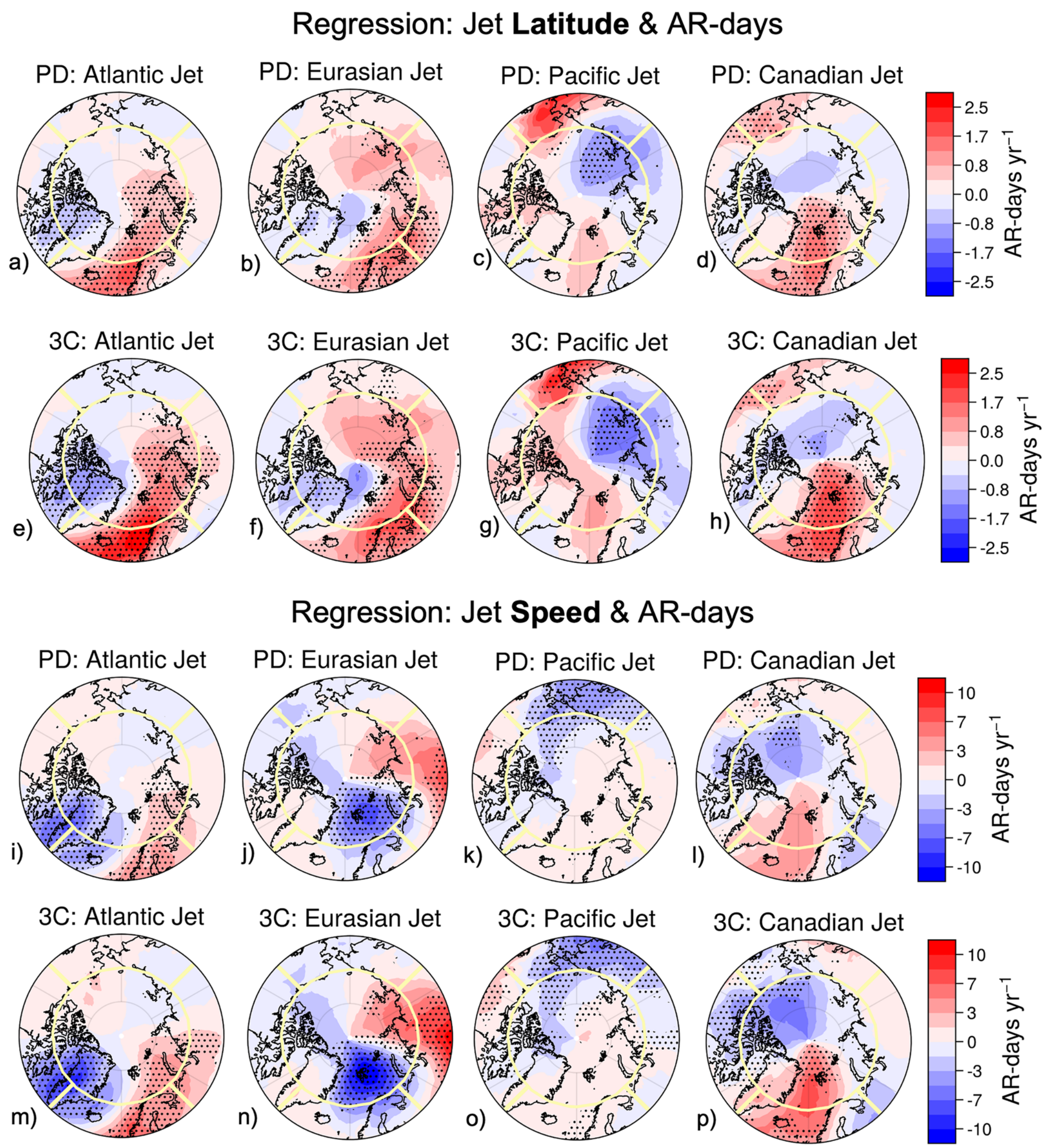

Figure 11. Above: Annual mean of seasonal regressions of the jet latitude in each sector with local atmospheric river (AR)-days for the present-day (PD) (a–d) and 3C (e–h) climate. Dotted regions represent areas where the regression is significant (p-value < 0.05) in all seasons. Below: Same as above but for regional jet speeds. Yellow lines represent the 70°N latitude band and sector divisions. Color scales represent the change in the amount of AR-days per year that a 1° shift in latitude (a–h) or a 1 m s^{-1} change in wind speed (i–p) would induce.

It is important to note that these weak/non-existent mean shifts (a) do not imply that the dynamical behavior jet streams and storm tracks in the models are unaffected by global warming, and (b) are potentially "underestimated" in current GCMs due to potentially inaccurate sensitivities or parametrizations (e.g., too weak eddy feedback, Screen et al., 2022). In our EC-Earth simulations, the amount of ARs that reach the Arctic in any given year and season is strongly linked to the position of the jet stream. For most anomalous poleward locations and increased speed of the jet in any sector, we found a distinct spatial pattern of increased AR-days in the south-eastern part of this sector and the western part of the subsequent sector to the east. Hence, the amount of ARs reaching any Arctic region significantly depends on the jet location and speed southwest of the region. With increased ARs in a warmer climate, this relation strengthens, suggested by increased significance in affected regions north of 70°N.

3.3. Effect of ARs on Arctic Climate: Seasonal Regressions

This section discusses the effect of ARs on Arctic SAT, precipitation (PR), and SIC on interannual time scales. As a first step, we regressed sector-specific ARPMT (crossing 70°N) with 2D fields of the three variables. In Figure 12, we show annual means of seasonal regressions (i.e., regions where in all seasons the regression slope was significant). We generally see a fairly similar spatial pattern across seasons, with strongest regressions in winter (partly caused by our annual mean threshold which limits winter ARs, increasing the regression strength). Hence, we here present annually averaged regressions, and discuss seasonal differences in the following Section 3.3. We find that the region where ARs cross 70°N distinctly determines the local effect of ARs on PR, SAT, and SIC. This finding holds true for the warmer climate (3C), but in most cases (sectors and variables), the regression strength weakens (Figures 12e–12h, 12m–12p, and 12u–12x). We hypothesize that this is because ARs in 3C dominate total PMT and are based on the PD moisture threshold: some 3C ARs are therefore relatively weak, while 3C anomalies in SAT, PR, and SIC are relative to the 3C climate and therefore more "anomalous." This results in a reduced average sensitivity of the variables to ARs in 3C.

We find that ARs originating from all sectors accompany higher local SAT in the respective regions north of the sector. Most markedly, the regression results suggest that even a 100 kg m^{-1} s^{-1} increase in Eurasian ARPMT (less than half of 1-sigma) is associated with 5°C temperature anomalies over Northern Eurasia and nearby ocean waters (Figure 12b). However, the relationship between ARs and surface temperature variations is complex and not one-sided, as non-AR-related positive Arctic temperature anomalies also facilitate ARs to penetrate further north (P. Zhang et al., 2023). Our regressions thus solely validate the connection between higher surface temperatures and AR occurrences in distinct Arctic regions. Based on observational evidence, Hegyi and Taylor (2018) and You et al. (2021) have shown that Arctic ARs can cause higher SAT through increased downwelling longwave fluxes. While turbulent sensible heat fluxes may also warm the surface, the warm air transported by ARs increases the stability of the lower atmosphere, hindering the warm air aloft to reach the colder surface. Komatsu et al. (2018) found observational evidence that warm air masses transported by Siberian ARs glide up over the colder surface air over sea ice. This may explain why the effect of ARPMT on SAT is strongest for ARs originating from the Eurasian and Canadian sector (Figures 12b and 12d), which are dominantly transported to continental regions (i.e., the Northern Eurasian coastline and Greenland) instead of ocean waters.

The PR response to increased ARPMT via the Atlantic and Pacific sectors is similar to the SAT response: increased moisture transport results in increased PR in the respective Atlantic/Pacific ocean basins and is capable of reaching areas around the North Pole (Figures 12i and 12k). Interestingly, Arctic ARs entering from continental Eurasia are not only associated with increased PR in the Eurasian Arctic sector, but also decreased (increased) PR over Southeast Greenland (the Northeastern Atlantic). Patterns like these can be caused by changes in large-scale atmospheric modes such as the NAO (Feldstein, 2003); for example, Luo et al. (2016) showed that enhanced Ural blocking drives more moisture from Eurasia into the Arctic, and is also linked to a positive NAO mode (which would induce a North Atlantic PR pattern as in Figure 12j). Increased Canadian ARPMT results in increased PR over the West coast of Greenland and is associated with decreased PR over the East coast. Possible driving mechanisms include an enhanced GBH, which (due to the strengthened anticyclonic circulation) typically decreases PR over Southeast Greenland and the Northern Atlantic. Such interrelations highlight that simple correlations and regressions are not always representing direct impacts. However, we found a robust pattern of increased PR north of the respective sector with high ARPMT, where local PR can increase up to 300 mm $year^{-1}$ per 100 kg m^{-1} s^{-1} of ARPMT (as in the Eurasian sector; Figure 12j). Moreover, the significant impact of ARs on local PR has also been thoroughly studied over Antarctica (Gehring et al., 2022; Gorodetskaya et al., 2014; Maclennan et al., 2022; Wille et al., 2021). An additional analysis where we calculated the 100 most extreme PR and ARPMT events (not shown) revealed that between 32% and 46% of the most extreme seasonal ARPMT events occur in the same year as the most extreme PR events (in all seasons and both climates).

The effect on sea ice north of 70°N is relatively subtle, where the total amount of significantly affected regions is smaller compared to SAT and PR (Figure 12, lower panel). Similar to the two-sided AR-TAS relation, sea ice melting can not only be triggered by heating from above, but can also initially occur due to increased ocean temperatures or strong winds, and then induce increased temperatures through evaporation, possibly strengthening ARs (Bintanja & Selten, 2014; Lei et al., 2018; Liang et al., 2023; Mattingly et al., 2023; P. Zhang et al., 2023). We find that especially ARs from Eurasia are associated with 20% lower SIC in the Kara Sea (Figure 12r). We also see regions where the sea ice response is significantly positive, but our sector analysis suggests that this might not

10.1029/2023JD038926

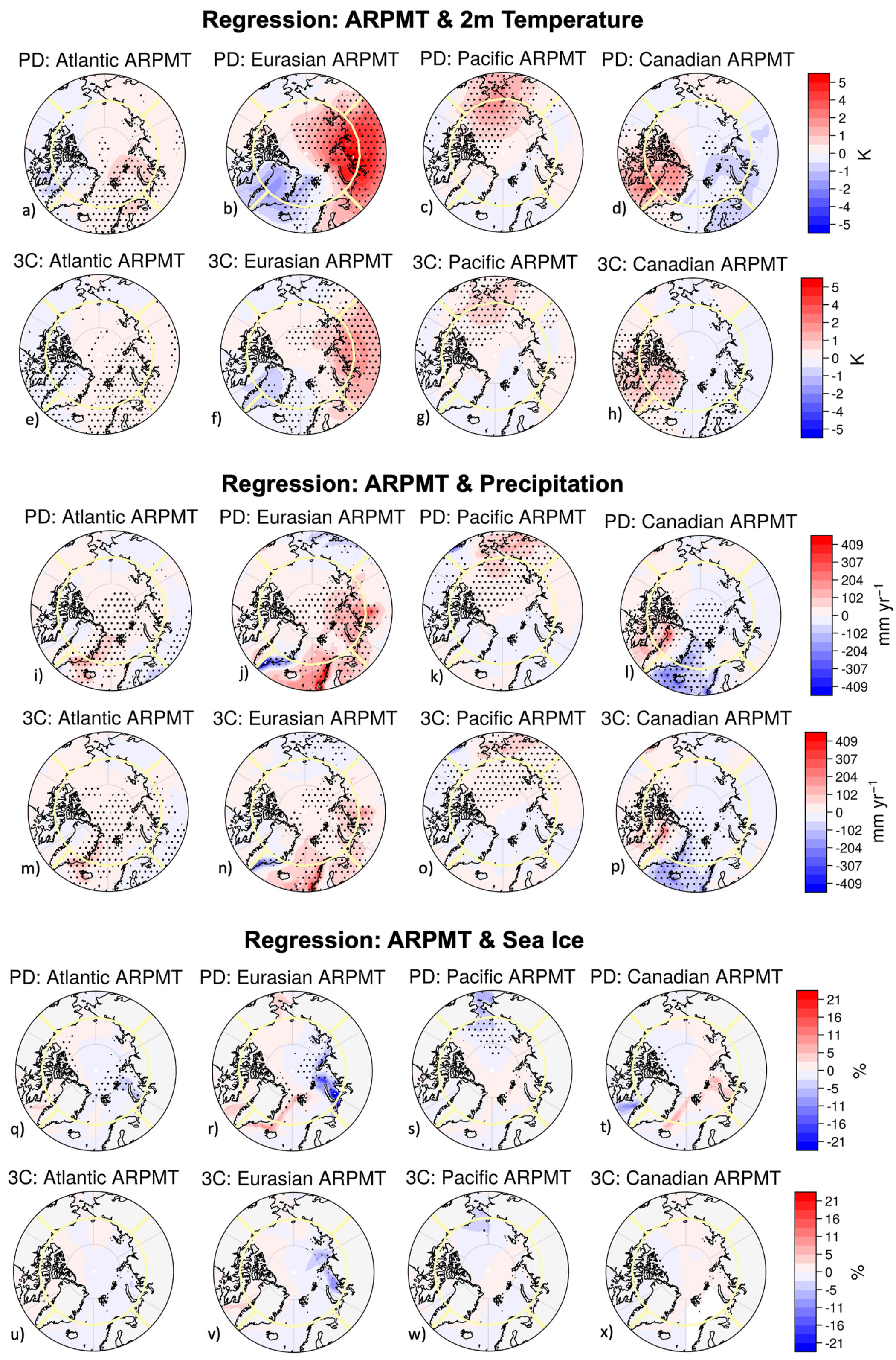

Figure 12. Annual mean of seasonal regressions of AR-related PMT (here in kg^{-100} m^{-1} s^{-1}) in each sector with local temperature (a–h), precipitation (i–p), and sea ice (q–x) for the present-day (PD) and 3C climate. Dotted regions represent areas where the regression is significant (p-value < 0.05) in all seasons. Yellow lines represent the 70°N latitude band and sector divisions.

represent a direct response to increased ARs; these positive sea ice anomalies are only found north and west of (a) Canada and (b) Greenland in years with anomalously high ARPMT from the (a) Atlantic and (b) Eurasian sector, instead of the (a) Canadian, and (b) Atlantic sector, from which the associated ARs would reach these regions. Rather, they may be indicators of climate mode variability. For example, higher SIC over Northern Canada during high Atlantic ARPMT years (Figure 12q) may be related to the positive phase of the NAO, which is associated with increased North Atlantic ARs (I. Benedict, Ødemark, et al., 2019) as well as increased SIC near Canada (Johnston et al., 2005; Qian et al., 2008).

To conclude, increased ARPMT is associated with higher SAT and PR directly north of the sector-dependent intrusions, and is dominantly linked to reduced sea ice in the respective regions. The PR response to ARs originating from the Atlantic, Eurasian, and Pacific sectors is significant even north of 80°N. The sector distinction of ARPMT offered a more robust evidence that the dominating effect on annual SIC is negative (i.e., high ARPMT is linked to reduced SIC). Note that season-specific or delayed sea ice responses to ARs (e.g., P. Zhang et al., 2023) are partly hidden in the annual average of seasonal regressions.

3.4. Caveats

This study contains a number of choices that potentially affect the results. We stress that all PD and future ARs are calculated using an annual-mean threshold. This allowed us to directly compare individual seasons, but implies that the absolute amount of ARs and ARPMT in each season could be considered as over- or underestimated considering the seasonally varying mean conditions. For example, due to lower moisture availability in colder seasons, we would capture more winter ARs when using a seasonal threshold, but they would carry significantly less moisture and may have less of an impact compared to summer ARs. Furthermore, our results are limited to the model-dependent representation of the PD and future climate in EC-Earth2.3, for example, modes of climate variability or the position and strength of the jet stream (I. Benedict, Ødemark, et al., 2019; Gao et al., 2015; C. Liu & Barnes, 2015; Ma et al., 2021; Neff, 2018). For example, the poleward shift in our Atlantic jet and ARs could be underestimated, as the PD North Atlantic jet in EC-Earth2.3 shows a poleward displacement compared to ERA5 (Döscher et al., 2022; Hazeleger et al., 2012). Lastly, the relation of ARs to Arctic climate as presented in this study is limited to a simple linear regression. Additional investigations of responsible processes could increase certainty about the direct effect of ARs on Arctic climate variations.

4. Conclusions

We evaluated Arctic ARs and moisture transport using long continuous coupled model simulations from EC-Earth2.3 to robustly investigate the influence of AR variability on Arctic climate. AR characteristics are comparable between ERA5 and the PD climate in EC-Earth. The application of a fixed relative as well as a relative method for the detection of future ARs allowed us to identify whether future AR changes are primarily caused by thermodynamic changes or are also dynamically driven.

First, we showed that the increase in total PMT variability is weak compared to the increase in mean PMT. Contrary results of other studies that imply a slight increase in the CoV of PMT are likely based on a simplified PMT calculation that includes EMT, which show opposite CoV trends to strictly northward PMT. Our results thus allude to a more consistent, less variable PMT to the Arctic, which is mainly caused by the strong increase in moisture transported by ARs. In a +3°C warmer than PI climate, 95% of the additional PMT is carried by ARs, increasing the total share of ARPMT to PMT from 42% to 53%. Correspondingly, the PMT carried by ARs becomes more consistent and less variable from year to year; scaling the IAV of ARPMT by its mean suggests a relative decrease in variability that is significant in all seasons and strongest in winter and spring. By distinguishing AR-intensity from AR-frequency, we showed that this decrease in ARPMT CoV is not caused by a less variable amount of moisture content per AR (intensity), but of AR-days per year (frequency). Simply put, Arctic AR-days are more consistent in warmer climates, but the transported moisture per AR will be highly variable.

The Arctic-wide mean increase in ARs in our 3C simulation is almost exclusively caused by significantly higher atmospheric moisture levels. Dynamical changes are merely of secondary importance in generating future AR changes, but can regionally amplify (as over the North Atlantic) or dampen (as over Greenland and most Arctic Ocean areas) the moisture-induced increase in ARs. However, we reiterate that dynamical responses strongly depend on the model-specific dynamic mean state and sensitivity to future warming. For example, the majority of additional ARs in the 3C simulations reach the Arctic from the Atlantic instead of the Pacific sector, which is likely a side effect of a poleward shift of the North Atlantic jet stream (as shown by more future AR-days in r3C).

The amount of ARs reaching any Arctic region in our simulations significantly depends on the jet location and speed southwest of the region. For most anomalous poleward locations and increased speed of the jet in any sector, we found a distinct spatial pattern of increased AR-days in the south-eastern part of this sector and the western part of the subsequent sector to the east. With increased ARs toward a warmer climate, this relation is strengthening, shown by increased significance in affected regions north of 70°N. We did not find strong changes in the mean latitude and speed of the jet stream in most seasons and sectors. However, these non-existing mean trends of jet latitude and speed may be incorrectly represented in most current GCMs, which also affect AR changes (Ma et al., 2021; Screen et al., 2022). Assuming a climate change-induced equatorward shift of the North Atlantic jet as suggested by Screen et al. (2022), more (less) ARs would reach Greenland (Northern Europe and the Barents and Kara Seas) (Figure 11). That said, mean changes in jet properties toward warmer climates may not be very noticeable due to strong interannual variations which are often linked to climate modes such as the NAO or the GBH (Barrett et al., 2020; I. Benedict, Ødemark, et al., 2019; J. J. Benedict, Clement, & Medeiros, 2019; Rimbu et al., 2007). Our results provide a reference for common jet-AR interactions and suggest that jet stream variability and AR occurrences are most robustly linked on a regional basis.

Increased ARPMT is strongly linked to higher local Arctic SAT and PR, as well as (moderate) reductions in local SIC. We have shown that the affected areas are mostly limited to the precise location of ARs (i.e., north of the respective sector of the AR "entrances"). This holds true for the PD as well as the 3C climate (in which regressions were even lower, probably in response to the increased consistency of ARs). Our results suggest that ARs originating from Eurasia have the strongest relation to Arctic climate variability, especially regarding SAT and SIC. While our results suggest that the relation between ARPMT and Arctic Climate variability does not strengthen toward future warming, the impacts of Arctic ARs in a warmer climate will likely be severe, as more precipitation will fall as rain, and increased temperatures and sea ice loss likely allow ARs to penetrate further north.

Appendix A

See Figures A1, A2, A3, and A4.

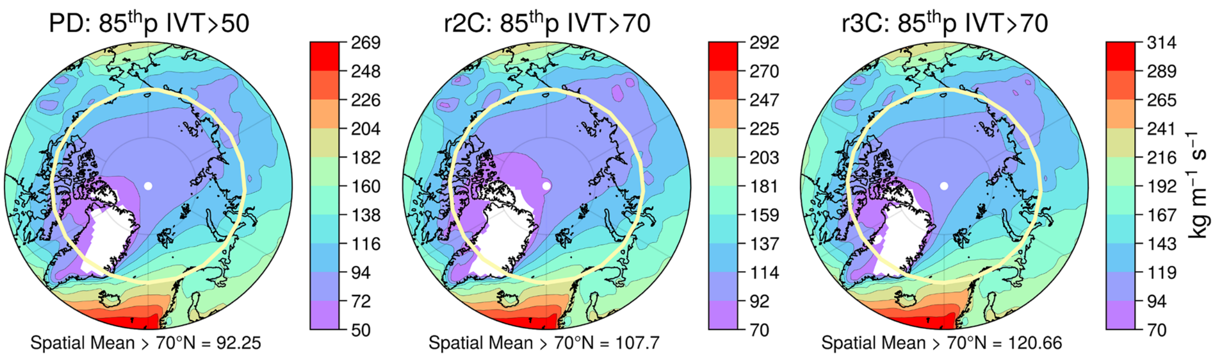

Figure A1. Mean integrated water vapor transport (IVT) in the EC-Earth present-day, 2 and 3C climates, plotted behind three different masks indicating the effect of the minimum IVT thresholds of 50 kg m^{-1} s^{-1} for the present-day climate and 70 kg m^{-1} s^{-1} for the future climates.

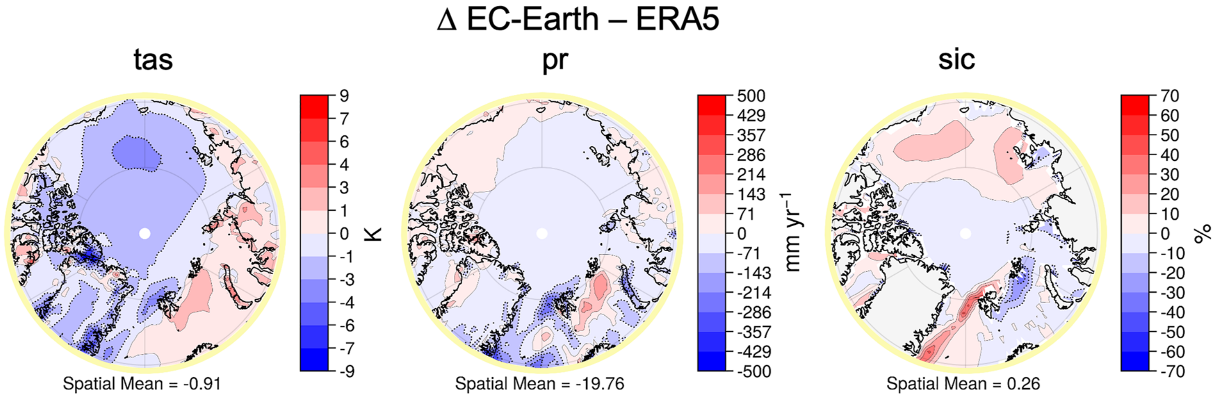

Figure A2. Spatial mean difference of annual surface air temperature, precipitation, and sea ice concentration north of 70°N between EC-Earth (present-day ensemble) and ERA5 (2005–2020).

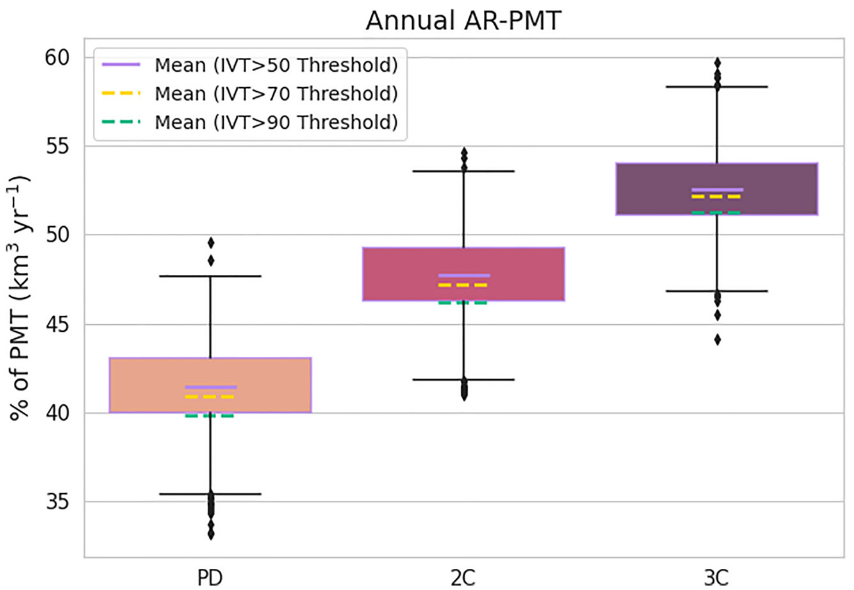

Figure A3. Annually averaged AR-related poleward moisture transport (ARPMT) and quartiles and outliers of the present-day (PD), +2°C warmer than PI (2C) and +3°C warmer than PI (3C) EC-Earth climate runs. The average % of ARPMT is also shown for the three different thresholds used.

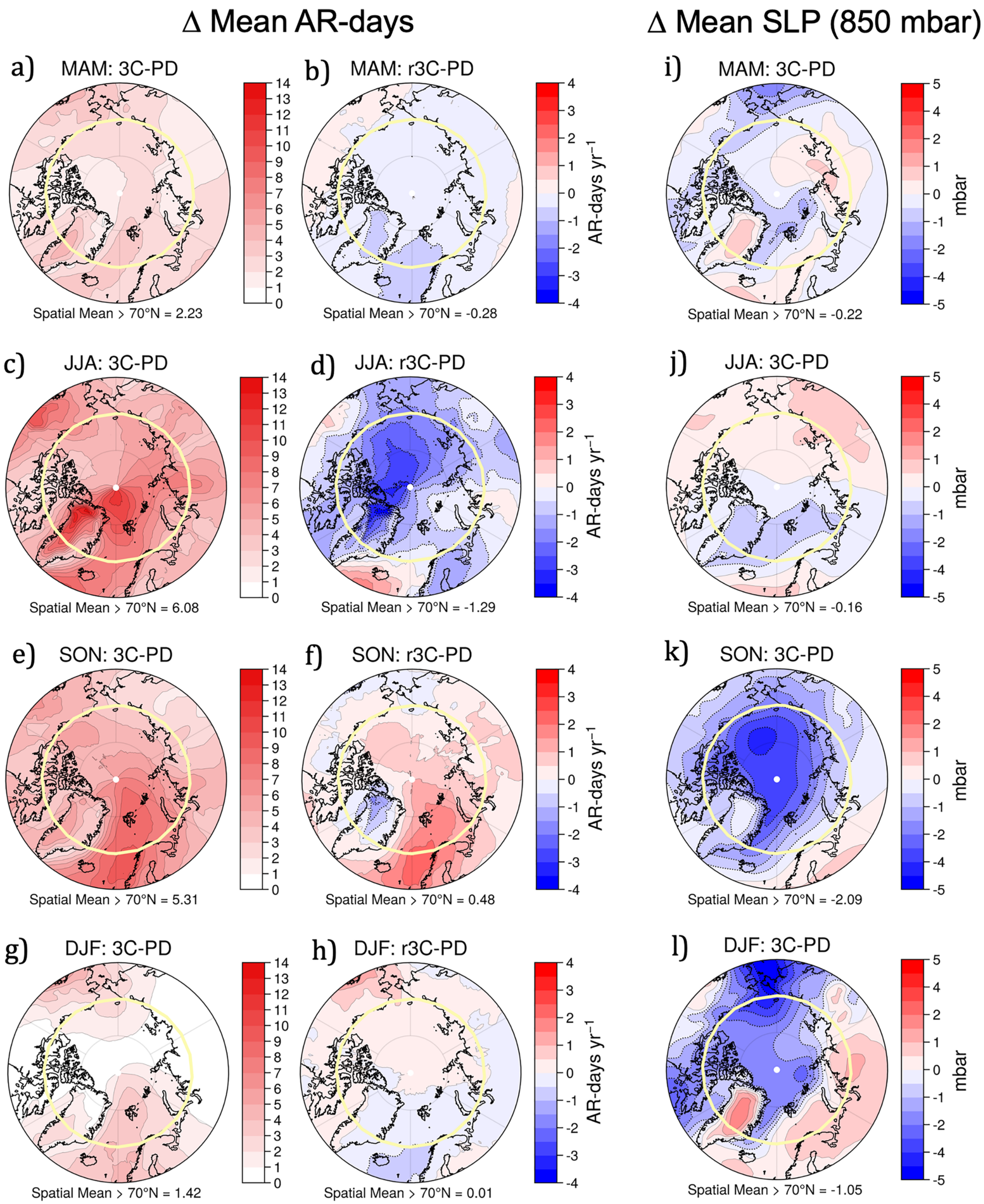

Figure A4. Left panel: Absolute (a, c, e, g) and dynamic-sensitive (b, d, f, h) change of AR-days from the present-day (PD) toward the 3C climate for each season. Right panel: Changes in sea level pressure at 850 mbar from the PD toward the 3C climate for each season (i–l).

Conflict of Interest

The authors declare no conflicts of interest relevant to this study.

Data Availability Statement

All EC-Earth simulation data and AR calculations can be obtained by contacting the author (marlen.kolbe@knmi.nl). The reanalysis product ERA5 is described in Hersbach et al. (2020) and publicly available at https://cds.climate.copernicus.eu/cdsapp#!/dataset/reanalysis-era5-pressure-levels?tab=overview.

Acknowledgments
We acknowledge the EC-Earth consortium for their contribution to the development of the EC-Earth climate model.

References

Allan, R. P., Liu, C., Zahn, M., Lavers, D. A., Koukouvagias, E., & Bodas-Salcedo, A. (2014). Physically consistent responses of the global atmospheric hydrological cycle in models and observations. *Surveys in Geophysics*, *35*(3), 533–552. https://doi.org/10.1007/s10712-012-9213-z

Bachand, C. L., & Walsh, J. E. (2022). Extreme precipitation events in Alaska: Historical trends and projected changes. *Atmosphere*, *13*(3), 388. https://doi.org/10.3390/atmos13030388

Bao, J., Michelson, S., Neiman, P., Ralph, F., & Wilczak, J. (2006). Interpretation of enhanced integrated water vapor bands associated with extratropical cyclones: Their formation and connection to tropical moisture. *Monthly Weather Review*, *134*(4), 1063–1080. https://doi.org/10.1175/mwr3123.1

Barnes, E. A., & Screen, J. A. (2015). The impact of Arctic warming on the midlatitude jet-stream: Can it? Has it? Will it? *Wiley Interdisciplinary Reviews: Climate Change*, *6*(3), 277–286. https://doi.org/10.1002/wcc.337

Barrett, B. S., Henderson, G. R., McDonnell, E., Henry, M., & Mote, T. (2020). Extreme Greenland blocking and high-latitude moisture transport. *Atmospheric Science Letters*, *21*(11), e1002. https://doi.org/10.1002/asl.1002

Benedict, I., Ødemark, K., Nipen, T., & Moore, R. (2019). Large-scale flow patterns associated with extreme precipitation and atmospheric rivers over Norway. *Monthly Weather Review*, *147*(4), 1415–1428. https://doi.org/10.1175/MWR-D-18-0362.1

Benedict, J. J., Clement, A. C., & Medeiros, B. (2019). Atmospheric blocking and other large-scale precursor patterns of landfalling atmospheric rivers in the North Pacific: A CESM2 study. *Journal of Geophysical Research: Atmospheres*, *124*(21), 11330–11353. https://doi.org/10.1029/2019jd030790

Bengtsson, L., Hodges, K. I., Koumoutsaris, S., Zahn, M., & Keenlyside, N. (2011). The changing atmospheric water cycle in Polar Regions in a warmer climate. *Tellus, Series A: Dynamic Meteorology and Oceanography*, *63*(5), 907–920. https://doi.org/10.1111/j.1600-0870.2011.00534.x

Bintanja, R., & Selten, F. M. (2014). Future increases in Arctic precipitation linked to local evaporation and sea-ice retreat. *Nature*, *509*(7501), 479–482. https://doi.org/10.1038/nature13259

Bintanja, R., van der Wiel, K., van der Linden, E. C., Reusen, J., Bogerd, L., Krikken, F., & Selten, F. M. (2020). Strong future increases in Arctic precipitation variability linked to poleward moisture transport. *Science Advances*, *6*(7), 1–7. https://doi.org/10.1126/sciadv.aax6869

Bogerd, L., van der Linden, E. C., Krikken, F., & Bintanja, R. (2020). Climate state dependence of Arctic precipitation variability. *Journal of Geophysical Research: Atmospheres*, *125*(8), e2019JD031772. https://doi.org/10.1029/2019JD031772

Chen, G., & Held, I. M. (2007). Phase speed spectra and the recent poleward shift of Southern Hemisphere surface westerlies. *Geophysical Research Letters*, *34*(21), L21805. https://doi.org/10.1029/2007gl031200

Collow, A. M., Shields, C. A., Guan, B., Kim, S., Lora, J., McClenny, E., et al. (2022). An overview of ARTMIP's Tier 2 reanalysis intercomparison: Uncertainty in the detection of atmospheric rivers and their associated precipitation. *Journal of Geophysical Research: Atmospheres*, *127*(8), e2021JD036155. https://doi.org/10.1029/2021jd036155

Döscher, R., Acosta, M., Alessandri, A., Anthoni, P., Arsouze, T., Bergman, T., et al. (2022). The EC-Earth3 Earth system model for the Coupled Model Intercomparison Project 6. *Geoscientific Model Development*, *15*(7), 2973–3020. https://doi.org/10.5194/gmd-15-2973-2022

Espinoza, V., Waliser, D. E., Guan, B., Lavers, D. A., & Ralph, F. M. (2018). Global analysis of climate change projection effects on atmospheric rivers. *Geophysical Research Letters*, *45*(9), 4299–4308. https://doi.org/10.1029/2017gl076968

Feldstein, S. B. (2003). The dynamics of NAO teleconnection pattern growth and decay. *Quarterly Journal of the Royal Meteorological Society*, *129*(589), 901–924. https://doi.org/10.1256/qj.02.76

Francis, D., Eayrs, C., Chaboureau, J.-P., Mote, T., & Holland, D. M. (2018). Polar jet associated circulation triggered a Saharan cyclone and derived the poleward transport of the African dust generated by the cyclone. *Journal of Geophysical Research: Atmospheres*, *123*(21), 11–899. https://doi.org/10.1029/2018jd029095

Francis, D., Fonseca, R., Nelli, N., Bozkurt, D., Picard, G., & Guan, B. (2022). Atmospheric rivers drive exceptional Saharan dust transport towards Europe. *Atmospheric Research*, *266*, 105959. https://doi.org/10.1016/j.atmosres.2021.105959

Francis, J. A., & Vavrus, S. J. (2015). Evidence for a wavier jet stream in response to rapid Arctic warming. *Environmental Research Letters*, *10*(1), 014005. https://doi.org/10.1088/1748-9326/10/1/014005

Gao, Y., Lu, J., Leung, L. R., Yang, Q., Hagos, S., & Qian, Y. (2015). Dynamical and thermodynamical modulations on future changes of landfalling atmospheric rivers over western North America. *Geophysical Research Letters*, *42*(17), 7179–7186. https://doi.org/10.1002/2015gl065435

Gehring, J., Vignon, É., Billault-Roux, A.-C., Ferrone, A., Protat, A., Alexander, S. P., & Berne, A. (2022). Orographic flow influence on precipitation during an atmospheric river event at Davis, Antarctica. *Journal of Geophysical Research: Atmospheres*, *127*(2), e2021JD035210. https://doi.org/10.1029/2021jd035210

Gimeno, L., Vázquez, M., Nieto, R., & Trigo, R. M. (2015). Atmospheric moisture transport: The bridge between ocean evaporation and Arctic ice melting. *Earth System Dynamics*, *6*(2), 583–589. https://doi.org/10.5194/esd-6-583-2015

Gimeno-Sotelo, L., Nieto, R., Vázquez, M., & Gimeno, L. (2019). The role of moisture transport for precipitation in the inter-annual and inter-daily fluctuations of the Arctic sea ice extension. *Earth System Dynamics*, *10*(1), 121–133. https://doi.org/10.5194/esd-10-121-2019

Gorodetskaya, I. V., Tsukernik, M., Claes, K., Ralph, M. F., Neff, W. D., & Van Lipzig, N. P. M. (2014). The role of atmospheric rivers in anomalous snow accumulation in East Antarctica. *Geophysical Research Letters*, *41*(17), 6199–6206. https://doi.org/10.1002/2014GL060881

Guan, B., & Waliser, D. E. (2015). Detection of atmospheric rivers: Evaluation and application of an algorithm for global studies. *Journal of Geophysical Research: Atmospheres*, *120*(24), 12514–12535. https://doi.org/10.1002/2015jd024257

Guo, Y., Shinoda, T., Guan, B., Waliser, D. E., & Chang, E. K. (2020). Statistical relationship between atmospheric rivers and extratropical cyclones and anticyclones. *Journal of Climate*, *33*(18), 7817–7834. https://doi.org/10.1175/jcli-d-19-0126.1

Hall, R., Erdélyi, R., Hanna, E., Jones, J. M., & Scaife, A. A. (2015). Drivers of North Atlantic polar front jet stream variability. *International Journal of Climatology*, *35*(8), 1697–1720. https://doi.org/10.1002/joc.4121

Hazeleger, W., Wang, X., Severijns, C., Stefanescu, S., Bintanja, R., Sterl, A., et al. (2012). EC-Earth V2.2: Description and validation of a new seamless Earth system prediction model. *Climate Dynamics*, *39*(11), 2611–2629. https://doi.org/10.1007/s00382-011-1228-5

Hegyi, B. M., & Taylor, P. C. (2018). The unprecedented 2016–2017 Arctic sea ice growth season: The crucial role of atmospheric rivers and longwave fluxes. *Geophysical Research Letters*, *45*(10), 5204–5212. https://doi.org/10.1029/2017GL076717

Hersbach, H., Bell, B., Berrisford, P., Hirahara, S., Horányi, A., Muñoz-Sabater, J., et al. (2020). Copernicus Climate Change Service (C3S) (2017): ERA5: Fifth generation of ECMWF atmospheric reanalyses of the global climate [Dataset]. Copernicus Climate Change Service Climate Data Store (CDS). https://doi.org/10.1002/qj.3803

Higgins, M. E., & Cassano, J. J. (2009). Impacts of reduced sea ice on winter Arctic atmospheric circulation, precipitation, and temperature. *Journal of Geophysical Research: Atmospheres*, *114*(D16), D16107. https://doi.org/10.1029/2009jd011884

Johnston, D., Friedlaender, A., Torres, L., & Lavigne, D. (2005). Variation in sea ice cover on the east coast of Canada from 1969 to 2002: Climate variability and implications for harp and hooded seals. *Climate Research*, *29*(3), 209–222. https://doi.org/10.3354/cr029209

Kidston, J., & Gerber, E. (2010). Intermodel variability of the poleward shift of the austral jet stream in the CMIP3 integrations linked to biases in 20th century climatology. *Geophysical Research Letters*, *37*(9), e1073. https://doi.org/10.1029/2010gl042873

Kim, B.-M., Hong, J.-Y., Jun, S.-Y., Zhang, X., Kwon, H., Kim, S.-J., et al. (2017). Major cause of unprecedented Arctic warming in January 2016: Critical role of an Atlantic windstorm. *Scientific Reports*, *7*(1), 1–9. https://doi.org/10.1038/srep40051

Kim, H.-M., & Kim, B.-M. (2017). Relative contributions of atmospheric energy transport and sea ice loss to the recent warm Arctic winter. *Journal of Climate*, *30*(18), 7441–7450. https://doi.org/10.1175/jcli-d-17-0157.1

Koenigk, T., Brodeau, L., Graversen, R. G., Karlsson, J., Svensson, G., Tjernström, M., et al. (2013). Arctic climate change in 21st century CMIP5 simulations with EC-Earth. *Climate Dynamics*, *40*(11), 2719–2743. https://doi.org/10.1007/s00382-012-1505-y

Komatsu, K. K., Alexeev, V. A., Repina, I. A., & Tachibana, Y. (2018). Poleward upgliding Siberian atmospheric rivers over sea ice heat up Arctic upper air. *Scientific Reports*, *8*(1), 1–15. https://doi.org/10.1038/s41598-018-21159-6

Lei, R., Cheng, B., Heil, P., Vihma, T., Wang, J., Ji, Q., & Zhang, Z. (2018). Seasonal and interannual variations of sea ice mass balance from the central Arctic to the Greenland Sea. *Journal of Geophysical Research: Oceans*, *123*(4), 2422–2439. https://doi.org/10.1002/2017jc013548

Liang, K., Wang, J., Luo, H., & Yang, Q. (2023). The role of atmospheric rivers in Antarctic sea ice variations. *Geophysical Research Letters*, *50*(8), e2022GL102588. https://doi.org/10.1029/2022gl102588

Light, B., Smith, M. M., Perovich, D. K., Webster, M. A., Holland, M. M., Linhardt, F., et al. (2022). Arctic sea ice albedo: Spectral composition, spatial heterogeneity, and temporal evolution observed during the MOSAiC drift. *Elementa: Science of the Anthropocene*, *10*(1), 000103. https://doi.org/10.1525/elementa.2021.000103

Liu, C., & Barnes, E. A. (2015). Extreme moisture transport into the Arctic linked to Rossby wave breaking. *Journal of Geophysical Research: Atmospheres*, *120*(9), 3774–3788. https://doi.org/10.1002/2014jd022796

Liu, Z., Risi, C., Codron, F., He, X., Poulsen, C. J., Wei, Z., et al. (2021). Acceleration of western Arctic sea ice loss linked to the Pacific North American pattern. *Nature Communications*, *12*(1), 1–9. https://doi.org/10.1038/s41467-021-21830-z

Luo, D., Xiao, Y., Yao, Y., Dai, A., Simmonds, I., & Franzke, C. L. (2016). Impact of Ural blocking on winter warm Arctic–cold Eurasian anomalies. Part I: Blocking-induced amplification. *Journal of Climate*, *29*(11), 3925–3947. https://doi.org/10.1175/jcli-d-15-0611.1

Ma, W., & Chen, G. (2022). What controls the interannual variability of the boreal winter atmospheric river activities over the Northern Hemisphere? *Journal of Climate*, *35*(23), 1–39. https://doi.org/10.1175/jcli-d-22-0089.1

Ma, W., Chen, G., Peings, Y., & Alviz, N. (2021). Atmospheric river response to Arctic sea ice loss in the polar amplification model intercomparison project. *Geophysical Research Letters*, *48*(20), e2021GL094883. https://doi.org/10.1029/2021gl094883

Maclennan, M. L., Lenaerts, J. T., Shields, C., & Wille, J. D. (2022). Contribution of atmospheric rivers to Antarctic precipitation. *Geophysical Research Letters*, *49*(18), e2022GL100585. https://doi.org/10.1029/2022gl100585

Mattingly, K. S., Mote, T., & Fettweis, X. (2018). Atmospheric river impacts on Greenland Ice Sheet surface mass balance. *Journal of Geophysical Research: Atmospheres*, *123*(16), 8538–8560. https://doi.org/10.1029/2018jd028714

Mattingly, K. S., Turton, J. V., Wille, J. D., Noël, B., Fettweis, X., Rennermalm, Å. K., & Mote, T. L. (2023). Increasing extreme melt in northeast Greenland linked to foehn winds and atmospheric rivers. *Nature Communications*, *14*(1), 1743. https://doi.org/10.1038/s41467-023-37434-8

Nash, D., Waliser, D., Guan, B., Ye, H., & Ralph, F. M. (2018). The role of atmospheric rivers in extratropical and polar hydroclimate. *Journal of Geophysical Research: Atmospheres*, *123*(13), 6804–6821. https://doi.org/10.1029/2017jd028130

Neff, W. (2018). Atmospheric rivers melt Greenland. *Nature Climate Change*, *8*(10), 857–858. https://doi.org/10.1038/s41558-018-0297-4

Nghiem, S., Rigor, I., Clemente-Colón, P., Neumann, G., & Li, P. (2016). Geophysical constraints on the Antarctic sea ice cover. *Remote Sensing of Environment*, *181*, 281–292. https://doi.org/10.1016/j.rse.2016.04.005

Notz, D., & Community, S. (2020). Arctic sea ice in CMIP6. *Geophysical Research Letters*, *47*(10), e2019GL086749. https://doi.org/10.1029/2019gl086749

O'Brien, T. A., Wehner, M. F., Payne, A. E., Shields, C. A., Rutz, J. J., Leung, L.-R., et al. (2022). Increases in future AR count and size: Overview of the ARTMIP Tier 2 CMIP5/6 experiment. *Journal of Geophysical Research: Atmospheres*, *127*(6), e2021JD036013. https://doi.org/10.1029/2021jd036013

Overland, J. E. (2021). Rare events in the Arctic. *Climatic Change*, *168*(3–4), 1–13. https://doi.org/10.1007/s10584-021-03238-2

Papritz, L., & Dunn-Sigouin, E. (2020). What configuration of the atmospheric circulation drives extreme net and total moisture transport into the Arctic. *Geophysical Research Letters*, *47*(17), e2020GL089769. https://doi.org/10.1029/2020gl089769

Payne, A. E., Demory, M. E., Leung, L. R., Ramos, A. M., Shields, C. A., Rutz, J. J., et al. (2020). Responses and impacts of atmospheric rivers to climate change. *Nature Reviews Earth & Environment*, *1*(3), 143–157. https://doi.org/10.1038/s43017-020-0030-5

Peings, Y., & Magnusdottir, G. (2014). Response of the wintertime Northern Hemisphere atmospheric circulation to current and projected Arctic sea ice decline: A numerical study with CAM5. *Journal of Climate*, *27*(1), 244–264. https://doi.org/10.1175/jcli-d-13-00272.1

Pendergrass, A. G., Knutti, R., Lehner, F., Deser, C., & Sanderson, B. M. (2017). Precipitation variability increases in a warmer climate. *Scientific Reports*, *7*(1), 1–9. https://doi.org/10.1038/s41598-017-17966-y

Qian, M., Jones, C., Laprise, R., & Caya, D. (2008). The influences of NAO and the Hudson Bay sea-ice on the climate of eastern Canada. *Climate Dynamics*, *31*(2–3), 169–182. https://doi.org/10.1007/s00382-007-0343-9

Ralph, F. M., Neiman, P. J., & Wick, G. A. (2004). Satellite and CALJET aircraft observations of atmospheric rivers over the eastern North Pacific Ocean during the winter of 1997/98. *Monthly Weather Review*, *132*(7), 1721–1745. https://doi.org/10.1175/1520-0493(2004)132<1721:sacaoo>2.0.co;2

Rimbu, N., Lohmann, G., & Grosfeld, K. (2007). Northern Hemisphere atmospheric blocking in ice core accumulation records from northern Greenland. *Geophysical Research Letters*, *34*(9), L09704. https://doi.org/10.1029/2006gl029175

Rivière, G. (2011). A dynamical interpretation of the poleward shift of the jet streams in global warming scenarios. *Journal of the Atmospheric Sciences*, *68*(6), 1253–1272. https://doi.org/10.1175/2011jas3641.1

Rutz, J. J., James Steenburgh, W., & Martin Ralph, F. (2014). Climatological characteristics of atmospheric rivers and their inland penetration over the western United States. *Monthly Weather Review*, *142*(2), 905–921. https://doi.org/10.1175/MWR-D-13-00168.1

Rutz, J. J., Shields, C. A., Lora, J. M., Payne, A. E., Guan, B., Ullrich, P., et al. (2019). The Atmospheric River Tracking Method Intercomparison Project (ARTMIP): Quantifying uncertainties in atmospheric river climatology. *Journal of Geophysical Research: Atmospheres*, *124*(24), 13777–13802. https://doi.org/10.1029/2019JD030936

Screen, J. A., Eade, R., Smith, D. M., Thomson, S., & Yu, H. (2022). Net equatorward shift of the jet streams when the contribution from sea-ice loss is constrained by observed eddy feedback. *Geophysical Research Letters*, *49*(23), e2022GL100523. https://doi.org/10.1029/2022gl100523

Screen, J. A., Simmonds, I., Deser, C., & Tomas, R. (2013). The atmospheric response to three decades of observed Arctic sea ice loss. *Journal of Climate*, *26*(4), 1230–1248. https://doi.org/10.1175/jcli-d-12-00063.1

Shields, C. A., & Kiehl, J. T. (2016). Atmospheric river landfall-latitude changes in future climate simulations. *Geophysical Research Letters*, *43*(16), 8775–8782. https://doi.org/10.1002/2016gl070470

Shields, C. A., Rutz, J. J., Leung, L. Y., Martin Ralph, F., Wehner, M., Kawzenuk, B., et al. (2018). Atmospheric River Tracking Method Intercomparison Project (ARTMIP): Project goals and experimental design. *Geoscientific Model Development*, *11*(6), 2455–2474. https://doi.org/10.5194/gmd-11-2455-2018

Skific, N., Francis, J. A., & Cassano, J. J. (2009a). Attribution of projected changes in atmospheric moisture transport in the Arctic: A self-organizing map perspective. *Journal of Climate*, *22*(15), 4135–4153. https://doi.org/10.1175/2009JCLI2645.1

Skific, N., Francis, J. A., & Cassano, J. J. (2009b). Attribution of seasonal and regional changes in Arctic moisture convergence. *Journal of Climate*, *22*(19), 5115–5134. https://doi.org/10.1175/2009jcli2829.1

Smith, D. M., Eade, R., Andrews, M., Ayres, H., Clark, A., Chripko, S., et al. (2022). Robust but weak winter atmospheric circulation response to future Arctic sea ice loss. *Nature Communications*, *13*(1), 1–15. https://doi.org/10.1038/s41467-022-28283-y

Sousa, P. M., Ramos, A. M., Raible, C. C., Messmer, M., Tomé, R., Pinto, J. G., & Trigo, R. M. (2020). North Atlantic integrated water vapor transport—From 850 to 2100 CE: Impacts on western European rainfall. *Journal of Climate*, *33*(1), 263–279. https://doi.org/10.1175/jcli-d-19-0348.1

Stroeve, J. C., Nandan, V., Willatt, R., Dadic, R., Rostosky, P., Gallagher, M., et al. (2022). Rain on snow (ROS) understudied in sea ice remote sensing: A multi-sensor analysis of ros during mosaic (multidisciplinary drifting observatory for the study of Arctic climate). *The Cryosphere*, *16*(10), 4223–4250. https://doi.org/10.5194/tc-16-4223-2022

Stroeve, J. C., Serreze, M. C., Holland, M. M., Kay, J. E., Malanik, J., & Barrett, A. P. (2012). The Arctic's rapidly shrinking sea ice cover: A research synthesis. *Climatic Change*, *110*(3), 1005–1027. https://doi.org/10.1007/s10584-011-0101-1

Tan, Y., Zwiers, F., Yang, S., Li, C., & Deng, K. (2020). The role of circulation and its changes in present and future atmospheric rivers over western North America. *Journal of Climate*, *33*(4), 1261–1281. https://doi.org/10.1175/jcli-d-19-0134.1

Tandon, N. F., Gerber, E. P., Sobel, A. H., & Polvani, L. M. (2013). Understanding Hadley cell expansion versus contraction: Insights from simplified models and implications for recent observations. *Journal of Climate*, *26*(12), 4304–4321. https://doi.org/10.1175/jcli-d-12-00598.1

van der Wiel, K., & Bintanja, R. (2021). Contribution of climatic changes in mean and variability to monthly temperature and precipitation extremes. *Communications Earth & Environment*, *2*(1), 1–11. https://doi.org/10.1038/s43247-020-00077-4

van der Wiel, K., Wanders, N., Selten, F. M., & Bierkens, M. F. P. (2019). Added value of large ensemble simulations for assessing extreme river discharge in a 2°C warmer world. *Geophysical Research Letters*, *46*(4), 2093–2102. https://doi.org/10.1029/2019GL081967

Vázquez, M., Algarra, I., Eiras-Barca, J., Ramos, A. M., Nieto, R., & Gimeno, L. (2018). Atmospheric rivers over the Arctic: Lagrangian characterisation of their moisture sources. *Water*, *11*(1), 1–14. https://doi.org/10.3390/w11010041

Wang, Z., Walsh, J., Szymborski, S., & Peng, M. (2020). Rapid Arctic sea ice loss on the synoptic time scale and related atmospheric circulation anomalies. *Journal of Climate*, *33*(5), 1597–1617. https://doi.org/10.1175/jcli-d-19-0528.1

Warner, M. D., & Mass, C. F. (2017). Changes in the climatology, structure, and seasonality of northeast Pacific atmospheric rivers in CMIP5 climate simulations. *Journal of Hydrometeorology*, *18*(8), 2131–2141. https://doi.org/10.1175/jhm-d-16-0200.1

Warner, M. D., Mass, C. F., & Salathé, E. P. (2015). Changes in winter atmospheric rivers along the North American west coast in CMIP5 climate models. *Journal of Hydrometeorology*, *16*(1), 118–128. https://doi.org/10.1175/jhm-d-14-0080.1

Webster, M. A., Parker, C., Boisvert, L., & Kwok, R. (2019). The role of cyclone activity in snow accumulation on Arctic sea ice. *Nature Communications*, *10*(1), 1–12. https://doi.org/10.1038/s41467-019-13299-8

Wille, J. D., Favier, V., Gorodetskaya, I. V., Agosta, C., Kittel, C., Beeman, J. C., et al. (2021). Antarctic atmospheric river climatology and precipitation impacts. *Journal of Geophysical Research: Atmospheres*, *126*(8), e2020JD033788. https://doi.org/10.1029/2020jd033788

Woods, C., Caballero, R., & Svensson, G. (2013). Large-scale circulation associated with moisture intrusions into the Arctic during winter. *Geophysical Research Letters*, *40*(17), 4717–4721. https://doi.org/10.1002/grl.50912

Woollings, T., Hannachi, A., & Hoskins, B. (2010). Variability of the North Atlantic eddy-driven jet stream. *Quarterly Journal of the Royal Meteorological Society*, *136*(649), 856–868. https://doi.org/10.1002/qj.625

Wu, Y., Ting, M., Seager, R., Huang, H.-P., & Cane, M. A. (2011). Changes in storm tracks and energy transports in a warmer climate simulated by the GFDL CM2.1 model. *Climate Dynamics*, *37*(1), 53–72. https://doi.org/10.1007/s00382-010-0776-4

Yim, B. Y., Min, H. S., & Kug, J.-S. (2016). Inter-model diversity in jet stream changes and its relation to Arctic climate in CMIP5. *Climate Dynamics*, *47*(1), 235–248. https://doi.org/10.1007/s00382-015-2833-5

You, C., Tjernström, M., & Devasthale, A. (2021). Warm-air advection over melting sea-ice: A Lagrangian case study. *Boundary-Layer Meteorology*, *179*(1), 99–116. https://doi.org/10.1007/s10546-020-00590-1

Zappa, G., Pithan, F., & Shepherd, T. G. (2018). Multimodel evidence for an atmospheric circulation response to Arctic sea ice loss in the CMIP5 future projections. *Geophysical Research Letters*, *45*(2), 1011–1019. https://doi.org/10.1002/2017gl076096

Zhang, P., Chen, G., Ma, W., Ming, Y., & Wu, Z. (2021). Robust atmospheric river response to global warming in idealized and comprehensive climate models. *Journal of Climate*, *34*(18), 7717–7734. https://doi.org/10.1175/jcli-d-20-1005.1

Zhang, P., Chen, G., Ting, M., Ruby Leung, L., Guan, B., & Li, L. (2023). More frequent atmospheric rivers slow the seasonal recovery of Arctic sea ice. *Nature Climate Change*, *13*(3), 1–8. https://doi.org/10.1038/s41558-023-01599-3

Zhang, X., He, J., Zhang, J., Polyakov, I., Gerdes, R., Inoue, J., & Wu, P. (2013). Enhanced poleward moisture transport and amplified northern high-latitude wetting trend. *Nature Climate Change*, *3*(1), 47–51. https://doi.org/10.1038/nclimate1631

Zhang, Z., Ralph, F. M., & Zheng, M. (2019). The relationship between extratropical cyclone strength and atmospheric river intensity and position. *Geophysical Research Letters*, *46*(3), 1814–1823. https://doi.org/10.1029/2018gl079071

Zhu, Y., & Newell, R. E. (1998). A proposed algorithm for moisture fluxes from atmospheric rivers. *Monthly Weather Review*, *126*(3), 725–735. https://doi.org/10.1175/1520-0493(1998)126<0725:apafmf>2.0.co;2